



HAL
open science

PRICKLE1 contributes to cancer cell dissemination through its interaction with mTORC2

Avais M Daulat, François Bertucci, Stéphane Audebert, Arnauld Sergé, Pascal Finetti, Emmanuelle Josselin, Rémy Castellano, Daniel Birnbaum, Stéphane Angers, Jean-Paul Borg

► **To cite this version:**

Avais M Daulat, François Bertucci, Stéphane Audebert, Arnauld Sergé, Pascal Finetti, et al.. PRICKLE1 contributes to cancer cell dissemination through its interaction with mTORC2 . *Developmental Cell*, 2016, 37, pp.311-325. 10.1016/j.devcel.2016.04.011 . hal-01321061

HAL Id: hal-01321061

<https://hal.science/hal-01321061>

Submitted on 25 May 2016

HAL is a multi-disciplinary open access archive for the deposit and dissemination of scientific research documents, whether they are published or not. The documents may come from teaching and research institutions in France or abroad, or from public or private research centers.

L'archive ouverte pluridisciplinaire **HAL**, est destinée au dépôt et à la diffusion de documents scientifiques de niveau recherche, publiés ou non, émanant des établissements d'enseignement et de recherche français ou étrangers, des laboratoires publics ou privés.

1 **PRICKLE1 contributes to cancer cell dissemination**
2 **through its interaction with mTORC2**

3
4 Avais M. Daulat^{1,2,3,4}, François Bertucci^{2,3,4,5}, Stéphane Audebert^{1,2,3,4}, Arnauld Serge^{2,3,4,6},
5 Pascal Finetti^{2,3,4,5}, Emmanuelle Josselin^{2,3,4,7}, Rémy Castellano^{2,3,4,7}, Daniel Birnbaum^{2,3,4,5},
6 Stéphane Angers^{8,9}, and Jean-Paul Borg^{1,2,3,4*}

7
8 ¹CRCM, Cell Polarity, Cell signalling and Cancer “Equipe labellisée Ligue Contre le Cancer”,
9 Inserm,U1068, Marseille, F-13009, France; ²Institut Paoli-Calmettes, Marseille, F-13009,
10 France; ³Aix-Marseille Université, F-13284, Marseille, France; ⁴CNRS, UMR7258; ⁵CRCM,
11 Molecular Oncology “Equipe labellisée Ligue Contre le Cancer”, Inserm, U1068, Marseille,
12 F-13009, France; ⁶CRCM, Leuko/Stromal Interactions, Inserm, U1068, Marseille, F-13009,
13 France ; ⁷CRCM, TrGET platform, Inserm,U1068, Marseille, F-13009, France; ⁸Department
14 of Pharmaceutical Sciences, Leslie Dan Faculty of Pharmacy, University of Toronto, Canada;
15 ⁹Department of Biochemistry, Faculty of Medicine, University of Toronto, Canada.

16
17 * To whom correspondence should be addressed: jean-paul.borg@inserm.fr /Phone 33-4-
18 8697-7201, Fax 33-4-8697-7499

19
20 **Running title:** PRICKLE1-mTORC2 complex controls cancer progression

23 **Summary**

24

25 Components of the evolutionarily conserved developmental planar cell polarity (PCP)
26 pathway were recently described to play a prominent role in cancer cell dissemination.
27 However, the molecular mechanisms by which PCP molecules drive the spread of cancer cells
28 remain largely unknown. *PRICKLE1* encodes a PCP protein bound to the promigratory
29 serine/threonine kinase MINK1. We identify RICTOR, a member of the mTORC2 complex,
30 as a PRICKLE1-binding partner and show that the integrity of the PRICKLE1-MINK1-
31 RICTOR complex is required for activation of AKT, regulation of focal adhesions and cancer
32 cell migration. Disruption of the PRICKLE1-RICTOR interaction results in a strong
33 impairment of breast cancer cell dissemination in xenograft assays. Finally, we show that up-
34 regulation of *PRICKLE1* in basal breast cancers, a subtype characterized by high metastatic
35 potential, is associated with poor metastasis-free survival.

36

37 **Keywords:** PRICKLE1, mTORC2, cancer cell migration, MINK1

38

39 **Introduction**

40 Recent data have revealed the importance of the PCP pathway in breast cancer dissemination
41 (Anastas et al., 2012; Belotti et al., 2013; Luga et al., 2012). This pathway is best known for
42 its physiological role in epithelial tissue morphogenesis during embryonic development of
43 invertebrates and vertebrates. The organization of PCP signaling relies on a set of
44 evolutionarily conserved molecules whose prominent members are *Wnts*, *Frizzled*, *Vang*
45 *Gogh*, *Flamingo*, *Dishevelled*, *Prickle* and *Diego* in *Drosophila* (Zallen, 2007). In vertebrates,
46 the homologous genes regulate convergent-extension cell movements during the early stages
47 of gastrulation, consisting of convergence of cells towards the midline, their intercalation
48 allowing the elongation of the antero-posterior body axis (Zallen, 2007). The PCP pathway
49 also regulates stereocilia alignment in neurosensory cells of the cochlea and epidermal
50 homeostasis (Narimatsu et al., 2009). In breast cancer, targeting this group of molecules using
51 silencing strategies has demonstrated its importance for cell motility and cancer
52 dissemination, in particular for *VANGL1*, the mammalian homologue of *Vang Gogh*, and its
53 associated molecules *DISHEVELLED*, *PRICKLE1*, and *FRIZZLED-2*, which constitutes a
54 potential target for antibody-based therapies (Anastas et al., 2012; Gujral et al., 2014).
55 Overexpression of *VANGL1*, *VANGL2* and *FRIZZLED2* has been consistently demonstrated
56 in breast cancer and correlates with tumor aggressiveness (Anastas et al., 2012; Gujral et al.,
57 2014; Puvirajesinghe et al., 2016).

58 *Prickle1* is known to regulate PCP in *Drosophila* (Gubb and Garcia-Bellido, 1982) as well as
59 convergent-extension in *Zebrafish* (Veeman et al., 2003) and *Xenopus* (Takeuchi et al., 2003).

60 *Prickle1* is conserved in evolution including in humans and encodes a protein containing an
61 amino-terminal Prickle Espinas Testis (PET) domain followed by three zinc finger-like
62 domains called LIM domains and a carboxy-terminal farnesylation site (**Fig. 2A**). Prickle
63 interacts with Vang Gogh in *Drosophila* (Jenny et al., 2003) and localizes asymmetrically at

64 the anterior pole during gastrulation and neurulation of polarized cells in *Zebrafish* (*Ciruna et*
65 *al.*, 2006). We have previously demonstrated that, in vertebrates, the asymmetric localization
66 of PRICKLE1 requires its phosphorylation by its binding partner MINK1, a Ste20-like
67 serine/threonine protein kinase involved in cell migration (Daulat et al., 2012) (Hu et al.,
68 2004). Recently, PRICKLE1 has been shown to play a role in the motility of MDA-MB-231
69 breast cancer cells and to be required for tumor progression in a xenograft mouse model
70 (Luga et al., 2012). However how it regulates cell motility and cancer cell dissemination
71 remains unknown.

72 Here we show that depletion of either PRICKLE1 or MINK1 in MDA-MB-231 cells
73 decreases cell motility by enhancing the formation of thick actin bundles and cell spreading.
74 We purified a set of PRICKLE1 interactors and identified a protein complex comprising
75 RICTOR, SIN1 and LST8, three members of the mTORC2 complex. The mTORC2 complex
76 phosphorylates and activates the serine-threonine kinase AKT through its interaction with the
77 serine-threonine kinase mTOR (Sarbasov et al., 2005). The mTOR-AKT pathway is crucial
78 for many cellular processes including cell migration (Zoncu et al., 2011) and plays a pivotal
79 role in tumor progression and metastatic dissemination (Agarwal et al., 2013; Gulhati et al.,
80 2011; Kim et al., 2011; Lamouille et al., 2012; Zhang et al., 2010). We show that the
81 PRICKLE1-MINK1-mTORC2 complex controls the phosphorylation of AKT and contributes
82 to cancer cell migration *in vitro* and *in vivo*. The integrity of the complex is required for the
83 regulation of focal adhesion turnover, a crucial event controlling cell motility. We find that
84 up-regulation of *PRICKLE1* is associated with shorter metastasis-free survival in basal breast
85 cancers. Our data suggest that targeting the PRICKLE1-mTORC2 complex could constitute a
86 promising strategy to treat this disease.

87

88 **Results**

89 **PRICKLE1 and MINK1 are involved in breast cancer cell migration**

90 To investigate the role of PRICKLE1 in cancer cell motility, we knocked-down PRICKLE1
91 expression by two siRNAs in MDA-MB-231, a highly invasive basal breast cancer cell line
92 (Ahmed et al., 2012; Luga et al., 2012; Zhang et al., 2010) (**Fig. 1A**, left panel).
93 Downregulation was correlated with a strong decrease of cell migration in Boyden chamber
94 assays (**Fig. 1A**, right panel). Given that MINK1 binds to and phosphorylates PRICKLE1
95 (Daulat et al., 2012), we downregulated MINK1 in MDA-MB-231 cells (**Fig. 1B**, left panel)
96 and measured a strong decrease of cell motility (**Fig. 1B**, right panel). Downregulation of
97 PRICKLE1 and MINK1 also led to reduced cell proliferation (**Fig. 1C, 1D**), to increased cell
98 spreading (**Fig. 1E**) and to the formation of thick actin bundles (**Fig. S1A**). We also measured
99 the relative size of the cells using flow cytometry analysis based on forward scatter and we
100 observed an increase of the size of cells downregulated for PRICKLE1 and MINK1 compared
101 to cells treated with non-targeting siRNA (**Fig. S1B**). Both PRICKLE1- and MINK1-depleted
102 cells presented a flattened phenotype as judged by the larger diameter of the nucleus, an
103 increased cell surface (quantified in **Fig. 1F**), and the absence of lamellipodia, suggesting a
104 lack of cellular polarization. Using the same assays, we obtained similar results with two
105 other basal breast cancer cell lines (SUM159 and SKBR7) and one ER/PR-positive breast
106 cancer cell line (MCF7) (**Fig. S2**). We also stained MDA-MB-231 cells with anti-VINCULIN
107 antibody, a marker of focal adhesions (FAs), and phalloidin (**Fig. 1G**), and found larger FAs
108 in PRICKLE1- or MINK1- depleted cells which mainly localized at the tips of actin bundles
109 as compared to control cells (**Fig. 1G**). We measured the area of more than 390 FAs observed
110 in one experiment, which is representative of three independent experiments using two
111 independent siRNAs per gene (**Fig. 1H**). We found that downregulation of either PRICKLE1
112 or MINK1 increased the presence of active $\beta 1$ -integrin, a major component of FAs, at the cell

113 surface (**Fig. S3A**), which correlates with the presence of more mature FAs in **Fig. 1G**.
114 Biotinylation assays of cell surface proteins showed a decreased internalization of β 1-integrin
115 in PRICKLE1- or MINK1-depleted cells (**Fig. S3B** and **S3C**). Our findings indicate that
116 PRICKLE1 and MINK1 regulate FA stabilization, integrin recycling and therefore actin
117 cytoskeleton organization and cell migration.

118

119 **Interaction of PRICKLE1 with MINK1 and phosphorylation of PRICKLE1 are** 120 **required for cell migration**

121 We previously showed that the second LIM domain of PRICKLE1 (LIM2) is required for the
122 interaction with MINK1 (**Fig. 2A**) (Daulat et al., 2012). We wondered whether the interaction
123 of PRICKLE1 with MINK1, and PRICKLE1 phosphorylation are important for cell
124 migration. We engineered MDA-MB-231 cells stably depleted for PRICKLE1 using two
125 independent shRNAs (**Fig. 2B**) and observed as with siRNAs (**Fig. 1A**) a decreased cell
126 migration proportional to knockdown efficiency (**Fig. 2B**). Cell migration was rescued by
127 expression of a VENUS-PRICKLE1 construct resistant to shRNA-PRICKLE1 (VENUS-
128 PRICKLE1 res) (**Fig. 2C**). To determine the contribution of the interaction between
129 PRICKLE1 and MINK1 in cell migration, we used a similar rescue strategy and expressed a
130 version of PRICKLE1 (VENUS-PRICKLE1 Δ LIM2) unable to bind MINK1 or a version of
131 PRICKLE1 (VENUS-PRICKLE1 P mutant) resistant to MINK1 phosphorylation in MDA-
132 MB-231 cells expressing shRNA-PRICKLE1 (Daulat et al., 2012). These two constructs were
133 unable to rescue cell motility of PRICKLE1-deficient MDA-MB-231 cells (**Fig. 2D**),
134 suggesting that both the interaction between PRICKLE1 and MINK1, and PRICKLE1
135 phosphorylation are required for cell motility. Expression of all constructs was confirmed by
136 western blot analysis (**Fig. 2 B-D**).

137

138 **PRICKLE1 forms a complex with mTORC2 and MINK1**

139 To characterize the signaling pathway associated with the MINK1-PRICKLE1 complex, we
140 generated a HEK293T cell expressing FLAG-PRICKLE1 and performed anti-FLAG
141 immunoprecipitation followed by mass spectrometry analysis. Among the identified proteins,
142 in addition to MINK1, we found that RICTOR, SIN1 and LST8, three members of the
143 mTORC2 complex, co-purified with PRICKLE1 (**Fig. 3A**). As RICTOR, SIN1 and LST8 are
144 associated with mTOR, a serine-threonine kinase responsible for the phosphorylation of AKT
145 (Sarbasov et al., 2005), we assessed its interaction with FLAG-PRICKLE1. Anti-FLAG
146 immunoprecipitation confirmed the presence of endogenous RICTOR and mTOR in the
147 PRICKLE1 complex (**Fig. 3B**). We also confirmed this interaction in MDA-MB-231 cells
148 stably expressing VENUS-PRICKLE1 (**Fig. 3C**). mTORC1 and mTORC2 are protein
149 complexes with distinct substrate specificities due to the presence of the RAPTOR and
150 RICTOR subunits, respectively. In HEK293T cells, FLAG-PRICKLE1 was able to co-
151 immunoprecipitate with Myc-RICTOR, but not with Myc-RAPTOR, confirming the specific
152 interaction of PRICKLE1 with the mTORC2 complex. We then asked whether MINK1
153 belongs to the PRICKLE1-RICTOR complex. We immunopurified FLAG-MINK1 from
154 HEK293T cells and observed a weak but reproducible MINK1-RICTOR co-purification (**Fig.**
155 **3E**, lane 1), which was increased by overexpression of VENUS-PRICKLE1 (**Fig. 3E**, lane 2),
156 suggesting that the MINK1-RICTOR interaction is dependent on the presence of PRICKLE1.
157 To prove this, we downregulated PRICKLE1 with two independent siRNAs and looked for
158 the presence of RICTOR in immunoprecipitated FLAG-MINK1 (**Fig. 3F**). The interaction
159 between MINK1 and RICTOR (**Fig. 3F**, lanes 1 and 2) was decreased upon PRICKLE1
160 downregulation (**Fig. 3F**, lanes 3 and 4). We next asked if MINK1 modulates the interaction
161 between PRICKLE1 and RICTOR. We immunopurified a mutant form of PRICKLE1 lacking
162 its MINK1 interaction domain (PRICKLE1 Δ LIM2) and observed a weaker RICTOR

163 interaction (**Fig. 3G**, compare lanes 2 and 3). Accordingly, overexpression of FLAG-MINK1
164 increased the interaction between VENUS-PRICKLE1 and endogenous RICTOR (**Fig. 3H**,
165 compare lanes 1 and 3). Expression of a kinase deleted MINK1 reduced this interaction (**Fig.**
166 **3H**, compare lanes 2 and 3). Finally, expression of VENUS-PRICKLE1 T370D, a
167 phosphomimetic mutant of PRICKLE1, in MDA-MB-231 cells led to an increased interaction
168 between PRICKLE1 and RICTOR compared to expression of VENUS-PRICKLE1 (**Fig. 3I**,
169 compare lanes 2 and 3). PRICKLE1 phosphorylation by MINK1 thus positively regulates the
170 interaction between PRICKLE1 and RICTOR. Like mTOR and RICTOR (McDonald et al.,
171 2008), FLAG-MINK1 localized at the lamellipodia (**Fig. 3J**). Moreover, we observed
172 colocalization of RICTOR and VENUS-PRICKLE1 at the lamellipodia of MDA-MB-231
173 cells (**Fig. 3K**, upper panels). Downregulation of MINK1 led to delocalization of PRICKLE1
174 from the cell cortex as previously shown in *Xenopus* cells (Daulat et al., 2012), as well as that
175 of RICTOR (**Fig. 3K**, lower panels). We quantified the decreased PRICKLE1/RICTOR
176 colocalization in the absence of MINK1 by counting the cells harboring cytoskeleton
177 modification seen in **Fig. 1G** as a marker of MINK1 downregulation (**Fig. 3L** and **Fig. 3M**).
178 Altogether these data suggest evidence that MINK1 controls PRICKLE1-dependent
179 recruitment of the mTORC2 complex at the leading edge of migratory cells where it regulates
180 actin cytoskeleton organization (**Fig. 3N**).

181

182 **Stability of focal adhesions is increased by targeting the PRICKLE1-mTORC2 complex**

183 Previous works had shown the involvement of MINK1 and mTORC2 in the modulation of
184 actin cytoskeleton organization (Hu et al., 2004; Lamouille et al., 2012; Sarbassov et al.,
185 2004). Consistent with these studies, we found that downregulation of RICTOR in MDA-MB-
186 231 cells led to actin cytoskeleton reorganization (**Fig. S1A**), decreased cell migration and
187 increased of cell spreading, and FA area (**Fig. S4A-F**), **increase of relative cell size using flow**

188 cytometry (**Fig. S1B**), and alteration of integrin endocytosis (**Fig. S3**), as observed for
189 PRICKLE1 and MINK1 downregulation (**Fig. 1** and **S3**). Migratory cells have two major
190 populations of FAs, nascent and mature, when adhering to extracellular matrices. Nascent
191 FAs present in the lamellipodia are highly dynamic and short lived. Some of these nascent
192 FAs mature following binding to actin filaments and ROCK activation, and appear as stable
193 patches at the plasma membrane (Burrige and Chrzanowska-Wodnicka, 1996; Parsons et al.,
194 2010). As depletion of PRICKLE1 or MINK1 increases the proportion of large, potentially
195 mature, FAs in MDA-MB-231 cells (**Fig. 1G**), we monitored the stability of FAs by Total
196 Internal Resonance Fluorescence (TIRF) microscopy, a well-suited method for the analysis of
197 dynamic events at the plasma membrane. MDA-MB-231 cells stably expressing VENUS-
198 PAXILLIN, a marker of FAs (Ahmed et al., 2012), seeded on collagen were downregulated
199 for PRICKLE1, MINK1 or RICTOR and the FA patches were followed over a period of 11
200 minutes. **Fig. 4A** (upper panels) shows a typical image of migratory MDA-MB-231 cells in
201 which FAs were localized every minute from 1 minute (red) to 11 minutes (purple) and each
202 FA was tracked and processed by a Matlab-based tracking software (Salles et al., 2013) (**Fig.**
203 **4A**, lower panels). Stable (mature) FAs were circled in white and were present throughout the
204 11 min acquisition. Transient FAs were considered unstable (nascent, circled in black) since
205 they appear or disappear within 11 min. Cells transfected with a control siRNA (siRNA NT)
206 had 20±3% of stable FAs whereas the proportion of stable FAs rose in MINK1- (34± 2%),
207 PRICKLE1- (38± 4%) and RICTOR- (32± 4%) depleted cells (**Fig. 4B**). We also monitored
208 the disassembly of FAs by determining the half-life of these structures: downregulation of
209 PRICKLE1, MINK1 and RICTOR led to stabilization of FAs whose half-life was increased
210 from 6.9 min (siRNA NT) to 8.2 min (siRNA PRICKLE1 or siRNA MINK1) and to 7.6 min
211 (siRNA RICTOR) (**Fig. 4C**). We also assessed PAXILLIN phosphorylation at Tyrosine 118,
212 a marker of mature FAs (Schaller and Parsons, 1995). Increased phosphorylation was

213 observed in PRICKLE1, MINK1 or RICTOR depleted cells confirming the conclusion of the
214 TIRF experiments (**Fig. 4D**). Our results reveal that the PRICKLE1-MINK1-RICTOR
215 complex controls cell migration of cancer cells by interfering with FA dynamics.

216

217 **The PRICKLE1 complex regulates mTORC2 activity**

218 As AKT is a substrate for mTORC2, we asked whether PRICKLE1 contributes to AKT
219 phosphorylation. In MDA-MB-231 cells, AKT phosphorylation monitored using specific anti-
220 phosphoSerine 473 (pS473-AKT) and anti-Threonine 308 (pT308-AKT) antibodies was
221 maximal after 30 min of serum treatment (**Fig. 5A**). AKT phosphorylation at both sites was
222 decreased upon PRICKLE1 downregulation (**Fig. 5B**). We did not observe an obvious
223 modification of phosphorylation of AKT at Threonine 450 or PKC α at Serine 657 suggesting
224 site- and substrate-specificities of the PRICKLE1-mTORC2 complex. Because the
225 phosphomimetic mutant of PRICKLE1 (T370D) improved PRICKLE1-RICTOR association
226 (**Fig. 3I**), we examined its effect on AKT phosphorylation. Although overexpression of
227 PRICKLE1 increased AKT phosphorylation at Serine 473 compared to the control,
228 overexpression of PRICKLE1 T370D was slightly more potent (**Fig. 5C**). We next examined
229 to what extent MINK1 contributes to AKT phosphorylation and found a strong reduction of
230 AKT phosphorylation in the absence of MINK1 (**Fig. 5D**). As for PRICKLE1 knockdown
231 (**Fig. 5B**), phosphorylation of AKT on Threonine 450 or of PKC α at Serine 657 was not
232 altered by MINK1 depletion (**Fig. 5D**). Cell motility of the highly invasive MDA-MB-231
233 cells was not increased by overexpressing either PRICKLE1 or PRICKLE1 T370D (data not
234 shown). We thus used SKBR7, another basal breast cancer cell line expressing lower levels of
235 PRICKLE1 (2.75 fold less *PRICKLE1* mRNA levels than MDA-MB-231 cells as measured
236 by Q-PCR) and presenting lower invasive properties. Downregulation of PRICKLE1 and
237 MINK1 decreased SKBR7 cell motility and led to actin skeleton reorganization (**Fig. S2**), and

238 decreased AKT phosphorylation (**Fig. S5A**). Conversely, overexpression of PRICKLE1 or
239 PRICKLE1 T370D increased AKT phosphorylation, cell motility and cell proliferation of
240 SKBR7 cells (**Fig. S5B-D**). Obviously, PRICKLE1 T370D was more potent than wild type
241 PRICKLE1 in these assays. These results provide evidence of the importance of PRICKLE1
242 in mediating mTORC2 activity and function.

243 We next purified FLAG-PRICKLE1 from HEK293T cells and performed *in vitro* kinase
244 assays using recombinant GST-AKT as a substrate. The PRICKLE1 complex promoted AKT
245 phosphorylation (**Fig. 5E**, lane 1) in comparison with a control RADIL complex (**Fig. 5E**,
246 lane 2). To test whether this event was due to the presence of the mTORC2 complex
247 associated with PRICKLE1, we downregulated RICTOR expression using two independent
248 shRNAs (**Fig. 5F**). Purification of the PRICKLE1 complex from these cells and incubation
249 with recombinant GST-AKT reduced AKT phosphorylation (**Fig. 5F**, lanes 2 and 3). The
250 PRICKLE1 complex thus contributes to AKT phosphorylation in living cells and *in vitro*.

251 MDA-MB-231 cells express two AKT forms (AKT1 and AKT2) whose phosphorylation was
252 decreased by PRICKLE1 downregulation (**Fig. 5G**). However, only AKT2 knockdown could
253 recapitulate the phenotype observed in PRICKLE1-depleted cells (actin cytoskeleton
254 reorganization, cell spreading and stabilization of FAs as revealed by vinculin staining) (**Fig.**
255 **5H, Fig. 5I**) although both AKT1 and AKT2 were efficiently depleted by specific shRNAs
256 (**Fig. 5J**). We also looked at the effects of specific inhibitors of AKT (MK2206) and MEK
257 (U0126) on MDA-MB-231 cells. With MK2206 (**Fig. 5K, 5L**), we observed increased cell
258 spreading and a remodeling of the cytoskeleton with the formation of thick actin bundles (**Fig.**
259 **S1D**) which phenocopied the results obtained upon PRICKLE1 or MINK1 downregulation
260 (**Fig. 1G, Fig. 1H, Fig. S1**). No such effects were found with U0126. However, in contrast to
261 the observation made with siRNAs directed against PRICKLE1, MINK1 and RICTOR (**Fig.**
262 **S1B**), we did not observe alteration of cell size under MK2206 treatment compare to control

263 by flow cytometry (**Fig. S1C**). The efficiency of the chemical treatments was assessed by
264 western blot using phosphorylation of AKT and of FOXO, a known AKT substrate, as
265 readouts (**Fig. 5M**). We thus conclude that PRICKLE1 can promote AKT phosphorylation
266 through its interaction with MINK1 and mTORC2.

267

268 **Interaction between PRICKLE1 and mTORC2 is required for AKT phosphorylation** 269 **and cell migration**

270 We next determined the role of the PRICKLE1-mTORC2 interaction in AKT phosphorylation
271 and cell migration. We generated deleted versions of PRICKLE1 lacking the PET and/or the
272 LIM domains and a construct encompassing the PRICKLE1 C-terminus region only
273 (PRICKLE C2) (**Fig. 6A**). In HEK293T cells, we found that the PET and LIM domains were
274 dispensable for the interaction, and that the PRICKLE C2 construct was not able to bind
275 RICTOR (**Fig. 6B**). The region between the LIM3 domain and the PRICKLE C2 region is
276 thus likely involved in the interaction with RICTOR. We fused this region (hereafter named
277 C1 domain) to VENUS (VENUS-C1) and transiently expressed the construct in HEK293T
278 cells. VENUS-C1, but not VENUS, was able to co-immunoprecipitate with endogenous
279 RICTOR (**Fig. 6C**). We next expressed FLAG-PRICKLE1 together with VENUS or VENUS-
280 C1 in HEK293T cells and found that expression of VENUS-C1 led to a strong decrease of
281 PRICKLE1-RICTOR interaction, highlighting its dominant-negative effect (**Fig. 6D**).
282 Overexpression of VENUS-C1 in MDA-MB-231 cells led to a robust inhibition of AKT
283 phosphorylation (**Fig. 6E**) and cell migration (**Fig. 6F**). In addition, expression of VENUS-C1
284 phenocopied the increase of cell spreading (**Fig. 6G, 6H**) and actin cytoskeleton
285 reorganization (**Fig. S1E**) previously observed by downregulating PRICKLE1 (**Fig. 1E,**
286 **S1A**). In conclusion, disruption of the PRICKLE1-RICTOR interaction decreases AKT

287 phosphorylation and cell migration similarly to depletion of the PRICKLE1 complex
288 components.

289

290 **The MINK1-PRICKLE1-RICTOR complex plays a role in tumor growth and metastatic** 291 **dissemination**

292 We next aimed to assess the *in vivo* contribution of the PRICKLE1 complex in cancer cell
293 spreading. PRICKLE1 and RICTOR have been linked to tumor progression and dissemination
294 using MDA-MB-231 cells in xenograft experiments (Luga et al., 2012) (Zhang et al., 2010).
295 No such data were available for MINK1. We generated luciferase-positive MDA-MB-231
296 cells stably downregulated for MINK1 expression (**Fig. S6A**) and observed a decrease of cell
297 motility (**Fig. S6B**) and cell proliferation (**Fig. S6C**) as was observed with siRNAs (**Fig. 1B,**
298 **1D**). In orthotopic transplantation assays into the mammary fat pad of NOD/SCID/ γ c mice,
299 we found, after 33 days, a decrease of the primary tumor volume with MINK1-deficient
300 MDA-MB-231 cells compare to control cells (**Fig. S6D**). Whereas MDA-MB-231 control
301 cells (shRNA NT) invaded the lungs (**Fig. S6E**) and the livers (**Fig. S6G**), we observed a
302 lower invasion rate (fewer metastases or no metastases in the lungs and in the livers, see
303 quantification of bioluminescence in **Fig. S6F** and **Fig. S6H**) with MINK1-deficient MDA-
304 MB-231 cells. Taken together, these *in vivo* data demonstrate that, like PRICKLE1 (Luga et
305 al., 2012) and RICTOR (Zhang et al., 2010), MINK1 is involved in the metastatic
306 dissemination of MDA-MB-231 cells.

307 We next addressed the role of the PRICKLE1-RICTOR interaction in cancer dissemination *in*
308 *vivo* using VENUS or VENUS-C1 in MDA-MB-231 cells stably expressing firefly luciferase.
309 VENUS-C1 expression decreased cell proliferation (**Fig. 7A**) and AKT phosphorylation (data
310 not shown), and led to compromised *in vivo* tumor growth (**Fig. 7B**). Metastasis formation
311 was observed in the lungs of all mice of the control group (7 out of 7 mice), whereas only 3

312 out of 8 mice developed lung metastases when VENUS-C1 was expressed (Fig. 7C, 7E).
313 Comparable results were obtained when considering metastasis in the liver (7 out of 7 mice
314 for VENUS as compared to 2 out of 8 mice for VENUS-C1) (Fig. 7D, Fig. 7F). We also
315 performed tail vein injections of luciferase-positive MDA-MB-231 cells expressing dominant-
316 negative PRICKLE1 VENUS-C1 (vs VENUS alone) or shRNA MINK1 (vs shRNA control),
317 and monitored the dissemination of cancer cells in the mice. We observed that, upon
318 intravenous injection, MDA-MB-231 cells populate the lungs and that, after 2 or 3 weeks,
319 total luminescence (mostly in lungs) was statistically lower in mice injected with cells
320 transfected with VENUS-C1 (Fig. 7G, Fig. 7H) or shMINK1 (Fig. S6I, Fig. S6J) compared
321 to controls. This phenotype is likely the result of a combinatory decrease of tumor growth and
322 metastatic potential of MDA-MB-231 cells. In conclusion, we have demonstrated the
323 importance of the PRICKLE1-RICTOR association in tumor growth and metastatic
324 dissemination *in vivo*.

325

326 ***PRICKLE1* upregulation correlates with poor prognosis in basal breast cancer**

327 Breast cancer is classified in five major intrinsic molecular subtypes (luminal A and B, basal,
328 ERBB2-enriched, normal-like) (Perou et al., 2000; Sorlie et al., 2001). Breast cancer cell lines
329 are classified in luminal, basal or mesenchymal subtypes. We analyzed *PRICKLE1* mRNA
330 expression in publicly-available datasets of 45 breast cancer cell lines and 5,410 primary
331 invasive breast carcinomas. Basal/mesenchymal cell lines (N=19) showed higher *PRICKLE1*
332 expression level than luminal cell lines (N=17; $p=1.78E-02$, Student t-test; Fig. 7I), the
333 expression levels being similar between basal and mesenchymal cell lines ($p=0.95$, Student t-
334 test; data not shown). In clinical samples, *PRICKLE1* expression level, measured as
335 continuous value, was also higher in basal breast cancers than in luminal A, luminal B and
336 ERBB2-enriched breast cancers (Fig. S7A, Fig. 7J; Supplementary Table 1). We then

337 searched for correlation between *PRICKLE1* expression (as binary variable) and
338 clinicopathological features of breast cancers, including metastasis-free survival (MFS).
339 Within the 5,410 breast cancer samples analyzed, 860 tumors (16%) showed *PRICKLE1*
340 upregulation when compared to normal breast (ratio T/NB ≥ 2 ; “*PRICKLE1*-up” group), and
341 4,550 (84%) did not show any upregulation (ratio < 2 ; “*PRICKLE1*-no up” group).
342 Correlations were found between “*PRICKLE1*” status and age of the patient ($p < 0.001$),
343 pathological type ($p < 0.001$), axillary lymph node status ($p = 0.049$), and grade ($p = 0.007$), ER
344 status ($p < 0.001$), PR status ($p < 0.001$), ERBB2 status ($p = 0.009$), and molecular subtypes
345 ($p < 0.001$) (**Supplementary Table 2**). MFS data were available for 1,037 patients, including
346 613 who remained metastasis-free during a median follow-up of 83 months and 424 who
347 displayed metastatic relapse. The 5-year MFS rate was 61% [95CI, 58-65]. In the whole
348 population, *PRICKLE1* upregulation was not associated with MFS ($p = 0.49$, log-rank test).
349 The same analysis was done in each molecular subtype separately. As shown in **Fig. 7K**, in
350 the basal subtype, *PRICKLE1* upregulation was associated with shorter 5-year MFS (41%
351 [95CI, 31-55] when compared with the “*PRICKLE1*-no up” group (61%, [95CI, 54-68];
352 $p = 0.008$; log-rank test). By contrast, no correlation with MFS was seen in the luminal A,
353 luminal B, ERBB2-enriched, and normal-like subtypes (data not shown). We next used
354 publicly available data sets to look for a possible correlation between *PRICKLE1* mRNA
355 expression and AKT activation. Among the 534 breast cancer samples from the TCGA
356 dataset (<https://tcga-data.nci.nih.gov/tcga/>), 368 had available data from reverse-phase protein
357 array (RPPA), allowing us to assess the expression of both AKT and activated AKT (pS473
358 and pT308 phosphorylated forms) and their correlation with *PRICKLE1* mRNA expression.
359 In the whole series of 368 samples, AKT expression was not associated with *PRICKLE1*
360 expression, whereas expression of each phosphorylated form was (pS473, $p < 0.001$; pT308,
361 $p < 0.001$; **Fig. S7B**). The same analysis limited to the basal subtype (N=85) showed similar

362 correlations, with higher expression of phosphorylated AKT in the *PRICKLE1*-up samples
363 than in the “*PRICKLE1*-no up” (pS473, p=0.015; pT308, p<0.001; **Fig. 7L**), suggesting a
364 positive correlation between *PRICKLE1* expression and AKT activation. Interestingly, in
365 basal breast cancers, *PRICKLE1* expression was also correlated to levels of phosphorylated
366 forms of FOXO3A and PRAS40, two downstream components of AKT signaling (**Fig. 7L**),
367 but not to phosphorylated MAPK and JNK (**Fig. S7C**). Together these data show
368 overexpression of *PRICKLE1* in basal breast cancer, its correlation with poor prognosis and
369 AKT signaling in this molecular subtype.

370 **Discussion**

371 Components of the evolutionary conserved group of developmental PCP genes play a pivotal
372 role in several aspects of cancer progression including cell proliferation, epithelial-
373 mesenchymal transition, cell migration and metastatic development. Overexpressed WNT5A
374 in breast cancer and melanoma contributes to enhanced cell migration and resistance to
375 treatment (Anastas et al., 2014; Dissanayake et al., 2007; Pukrop et al., 2006). Deregulation of
376 SCRIBBLE was observed in breast (Anastas et al., 2012) and prostate cancers (Pearson et al.,
377 2011), and found associated with increased cell proliferation and cell migration (Anastas et
378 al., 2012; Belotti et al., 2013). VANGL1 and VANGL2 are involved in cell motility,
379 proliferation and dissemination in breast cancer (Anastas et al., 2012; Belotti et al., 2013;
380 Luga et al., 2012; Puvirajesinghe et al., 2016). In addition, overexpression of SFRP1, an
381 inhibitor of the PCP pathway, limits cancer cell motility (Matsuda et al., 2009). Recently, high
382 levels of FRIZZLED2 and its ligand WNT5A were found in metastatic liver, lung, colon and
383 breast cancers (Gujral et al., 2014). This upregulation was correlated with epithelial-
384 mesenchymal transition and poor survival, and it was suggested that targeting this pathway
385 may benefit to cancer patients. At the molecular level, alterations of PCP components in
386 cancer lead to increased activation of important cell signaling pathways such as the RAS-
387 MAPK and Hippo pathways in the case of SCRIBBLE defects (Cordenonsi et al., 2011; Dow
388 et al., 2008) or the FYN-STAT3 pathways for WNT5A-FRIZZLED up-regulation (Gujral et
389 al., 2014).

390 Here we have studied PRICKLE1, a PCP component first described in *Drosophila* (Gubb and
391 Garcia-Bellido, 1982), known for its involvement in the metastatic potential of MDA-MB-231
392 breast cancer cell line (Luga et al., 2012). We have shown that PRICKLE1 and its partner
393 MINK1, as well as their interaction, are involved in cancer cell proliferation, migration and
394 actin cytoskeleton organization (**Fig. 1, Fig. 2**). In agreement with a previous report (Luga et

395 al., 2012), we observed that PRICKLE1 localizes at the leading edge of MDA-MB-231 cells
396 and provided evidence that this is a MINK1-dependent process (**Fig. 3K**). Previous studies
397 have shown that VANGL1 and VANGL2, two binding partners of PRICKLE1, are also
398 located at the leading edge of migratory cancer cells (Anastas et al., 2012; Belotti et al., 2013;
399 Luga et al., 2012).

400 We next purified PRICKLE1-associated partners by a proteomic approach and identified
401 RICTOR as an interactor (**Fig. 3**). RICTOR belongs to the mTORC2 complex that contains
402 mTOR (Jacinto et al., 2004; Sarbassov et al., 2004), which we found associated with
403 PRICKLE1. This finding highlights a connection between PRICKLE1, MINK1 and the
404 mTORC2 complex, which is important for AKT phosphorylation (Sarbassov et al., 2005),
405 actin cytoskeleton remodeling and cell migration (Jacinto et al., 2004; Sarbassov et al., 2004).

406 Two recent studies have demonstrated a connection between PCP core components, mTORC2
407 pathway, and AKT activation in melanoma and in muscles (Anastas et al., 2014; von
408 Maltzahn et al., 2012). We show that association of the mTORC2 complex with PRICKLE1 is
409 required for phosphorylation of AKT on Serine S473 in cells and *in vitro* (**Fig. 5**).

410 Phosphorylation of AKT at Serine 473 and Threonine 450 are required for signaling and
411 stability of AKT, respectively (Facchinetti et al., 2008). We did not find alteration of
412 phosphorylation of AKT at Threonine 450 and PKC α at Serine 657 when the expression of
413 PRICKLE1 or MINK1 was lost (**Fig. 5B** and **5D**) suggesting a role of the PRICKLE1
414 complex in AKT-mediated signaling. The involvement of MINK1 and mTORC2 in actin
415 cytoskeleton remodeling (Hu et al., 2004; Jacinto et al., 2004; Sarbassov et al., 2004) fits well
416 with our observation that these components, as well as PRICKLE1, play a role on FA
417 dynamics (**Fig. 1**, **Fig. 4**). We cannot exclude a role for RICTOR in cell migration
418 independently of mTORC2 as shown by others (Agarwal et al., 2013; Zhang et al., 2010).

419 However, downregulation of AKT2 and treatment with MK2206 recapitulated partially the

420 phenotypes we observed with loss of PRICKLE1, MINK1 and RICTOR expression (**Fig. 5H,**
421 **Fig. 5K**) suggesting a prominent role of AKT in the PRICKLE1-dependent pathway.
422 However, the fact that chemical inhibition of AKT (MK2206 treatment) did not change the
423 cell size by flow cytometry (Fig. S1C) and was less efficient than the absence of MINK1,
424 PRICKLE1, and RICTOR on cell spreading (Fig. 1E, F and Fig. 5K, L) cannot rule out the
425 additional implication of AKT-independent signaling events. It is also intriguing that whereas
426 both AKT1 and AKT2 phosphorylation was decreased by PRICKLE1 downregulation (**Fig.**
427 **5G**), only AKT2 loss gave rise to a PRICKLE1-like phenotype (**Fig. 5H**). Our study supports
428 the conclusion drawn by others about non-overlapping functions of AKT1 and AKT2 (Chin
429 and Toker, 2009). As RICTOR localized at the leading edge of MDA-MB-231 cells (**Fig. 3K**)
430 (McDonald et al., 2008), together with PRICKLE1 in a MINK1-dependent manner, we
431 propose a model whereby MINK1 controls PRICKLE1-mTORC2 localization at the leading
432 edge of migrating cells, a step necessary for local AKT phosphorylation by mTORC2 (**Fig.**
433 **3N**). We were not able to rescue loss of cell migration and cell proliferation of MINK1-
434 depleted cells by overexpression of PRICKLE1 or PRICKLE1 T370D. MINK1 is thus
435 required for PRICKLE1 functions, a result in agreement with our conclusion that interaction
436 between MINK1 and PRICKLE1 (and its phosphorylation by MINK1) represents a key step
437 for PRICKLE1 functions. Because MINK1 has probably other substrates than PRICKLE1, it
438 remains important to further study the mode of action of this protein kinase.

439 Novel AKT substrates such as Cortactin, a protein implicated in cell migration and invasion
440 (Wu et al., 2014), could be implicated in the control of actin cytoskeleton by the PRICKLE1-
441 mTORC2 complex. Indeed, Cortactin binds to the ARP2/3 complex and regulates actin
442 branching, polymerization during cell motility and FA dynamics (MacGrath and Koleske,
443 2012; Tomar et al., 2012). Previous work has shown that downregulation of mTOR and
444 RICTOR leads to reorganization of actin cytoskeleton (Sarbasov et al., 2004) and FAs

445 (Lamouille et al., 2012) in migrating cells. We confirmed these findings using an AKT
446 inhibitor and obtained similar effects by downregulation of the PRICKLE1 complex
447 components (**Fig. 1, Fig. 5**). To further determine the involvement of PRICKLE1 and its
448 binding partners in FA dynamics, we used TIRF experiments and observed that PRICKLE1,
449 MINK1 and RICTOR play a prominent role in FA stability (**Fig. 4**). Previous work has found
450 that RICTOR is associated with integrins and regulates AKT phosphorylation (McDonald et
451 al., 2008). Downregulation of PRICKLE1, MINK1 or RICTOR led to a defect of integrin
452 internalization and polarization (**Fig. S3**) linked to altered FA dynamics and decreased cell
453 migration (**Fig. 1, Fig. 4**). Interestingly, the *Drosophila* MINK1 ortholog, Misshapen (Msn),
454 similarly regulates integrin level at the cell surface which probably explains its promigratory
455 function (Lewellyn et al., 2013). A connection exists between the PCP pathway and FA
456 dynamics (Cui et al., 2013; Matsumoto et al., 2010; Wei et al., 2013). Indeed, WNT5A
457 promotes localization of FRIZZLED2 at the leading edge of migrating cells and triggers FAK
458 and PAXILLIN phosphorylation (Matsumoto et al., 2010). Furthermore, SYNDECAN4, a
459 membrane protein with PCP functions associated with FRIZZLED7 (Munoz et al., 2006) and
460 VANGL2 (Escobedo et al., 2013), regulates the formation of FAs through engagement of
461 $\alpha 5 \beta 1$ integrin (Saoncella et al., 1999) and, in endothelial cells, regulates mTORC2
462 localization and AKT (Partovian et al., 2008). As PRICKLE1 and MINK1 control
463 internalization and recycling of PCP receptors by a RAB5-dependent mechanism (Daulat et
464 al., 2012), we thus hypothesize that the PRICKLE1 complex could, directly or indirectly, play
465 such a role on integrins or other FA-associated molecules. Future studies will have to
466 determine how the PRICKLE1 complex regulates the functions of integrins.

467 We identified a region (C1) in PRICKLE1 required for its interaction with RICTOR and
468 showed that it behaves as a dominant-negative construct *in vitro* and *in vivo* (**Fig. 6** and **Fig.**
469 **7**) (Tao et al., 2009). Our (**Fig. S6**) and previously published (Luga et al., 2012) (Zhang et al.,

470 2010) data show that knockdown of MINK1, RICTOR or PRICKLE1 reduces the capacity of
471 breast cancer cells to invade secondary organs in xenograft experiments. In our previous
472 report, we concluded that only MINK1, and not its paralogs TNIK or MAP4K4, was
473 associated with PRICKLE1 (Daulat et al., 2012). MINK1 has been previously shown to
474 regulate HT1080 cell motility (Hu et al., 2004), a role apparently conserved during evolution
475 (Houalla et al., 2005). We propose a molecular mechanism whereby PRICKLE1 specifically
476 associates with MINK1, and contributes to cell motility *in vitro* and *in vivo*.

477 Using a large dataset of clinical primary invasive breast cancers, we found that *PRICKLE1* is
478 overexpressed in basal breast cancers where its up-regulation is correlated with poor
479 prognosis (**Fig. 7I-L, Fig. S7**). We also found that *PRICKLE1* mRNA upregulation in basal
480 breast cancers correlates with increased phosphorylation of AKT and its downstream
481 components (FOXO and PRAS40), but not with phosphorylated MAPK and JNK, which
482 nicely confirms our results obtained in cultured cells. No alteration of *MINK1* mRNA
483 expression was found in this series (data not shown). Targeted therapy has allowed a
484 significant improvement of patient outcome in breast cancers expressing ERBB2 or hormone
485 receptors. This is not the case for the basal subtype characterized by a high degree of cell
486 proliferation, metastatic development, and frequent relapse. Major efforts are thus required to
487 uncover novel markers and therapeutic targets for this poor prognosis cancer to improve
488 patients care. Targeting the AKT-mTOR pathway is a potential option to treat basal breast
489 cancers (Tao et al., 2014; Yunokawa et al., 2012). In our study, we have shown that inhibition
490 of PRICKLE1, MINK1 or RICTOR expression as well as disruption of the PRICKLE1-
491 RICTOR interaction decrease cell migration and tumor growth. Our findings may pave the
492 way to strategies able to inhibit or disrupt this complex that may benefit cancer patients.

493 **Acknowledgements**

494 The authors wish to thank Valérie Ferrier, Michael Sebbagh and Eric Bailly for critical review
495 of the manuscript and people from the cell imaging, cell sorting and animal house facilities.
496 This work was funded by La Ligue Nationale Contre le Cancer (Label Ligue JPB and DB, and
497 post-doctoral fellowship to AMD), Fondation de France (post-doctoral fellowship to AMD),
498 Fondation ARC pour la Recherche sur le Cancer (grant to JPB and AS), and SIRIC (INCa-
499 DGOS-Inserm 6038, fellowship to AMD). The Marseille Proteomics (IBiSA) and TrGET
500 platforms are supported by Institut Paoli-Calmettes (IPC) and Canceropôle PACA. Samples
501 of human origin and associated data were obtained from the IPC/CRCM Tumor Bank that
502 operates under authorization # AC-2013-1905 granted by the French Ministry of Research.
503 Prior to scientific use of samples and data, patients were appropriately informed and asked to
504 express their consent in writing, in compliance with French and European regulations. The
505 project was approved by the IPC Institutional Review Board. Jean-Paul Borg is a scholar of
506 Institut Universitaire de France.

507

508 **Figure Legends:**

509 **Figure 1: PRICKLE1 and MINK1 are involved in cell migration and cell proliferation of**
510 **MDA-MB-231 cells. A.** Loss of *PRICKLE1* mRNA expression was confirmed by quantitative
511 PCR (left panel). Transfected cells were subjected to a cell migration assay using Boyden
512 chambers (right panel). **B.** Same as (A) using two independent siRNAs targeting MINK1. **C-**
513 **D.** PRICKLE1 (C) and MINK1 (D) play a role in cell proliferation. Cell proliferation was
514 measured at the indicated times. **E.** Cell spreading of MDA-MB-231 treated with the
515 indicated siRNA. **F.** Quantification in (E). Cell spreading were measured using ImageJ
516 software. **G.** Same as (E) **H.** Sizes of focal adhesions were measured using vinculin staining
517 and ImageJ software analysis. One way ANOVA with Tukey post-test statistical analysis. *P
518 <0.05; **P<0.01; ***P<0.001. Data are presented as means \pm SEM. Scale bars are 20 μ M. See
519 also Figures S1, S2, S3.

520

521 **Figure 2: Interaction of PRICKLE1 with MINK1 is required for cell migration. A.**
522 Schematic representation of PRICKLE1. Phosphorylation (S324, S349, T370 and T795) and
523 the carboxy-terminal farnesylation (CIIS) sites are shown. **B.** Boyden chamber assays using
524 MDA-MB-231 cells (top panel). Downregulation of *PRICKLE* mRNA was confirmed by
525 semi-quantitative PCR (bottom panel). **C.** Rescue of PRICKLE1 expression in MDA-MB-231
526 cells followed by Boyden chamber assay. **D.** MDA-MB-231 cells stably expressing the
527 indicated PRICKLE1 mutants were subjected to shRNA treatment targeting PRICKLE1
528 (#405) and subjected to Boyden chamber assays. Protein expression was evaluated by western
529 blot with anti-GFP antibody. **B-D.** One way ANOVA with Tukey post-test statistical analysis.
530 ***P<0.001. Data are presented as means \pm SEM.

531

532 **Figure 3: PRICKLE1 forms a complex with RICTOR and mTOR.** **A.** Schematic
533 representation of the protein complex associated to PRICKLE1. Total Spectral Counts (TSCs)
534 is given for each member of the PRICKLE1 purified protein complex. **B.** In 293T cells,
535 FLAG-PRICKLE1 is associated with endogenous RICTOR and mTOR. **C.** MDA-MB-231
536 cells were transfected with VENUS-Ctrl or VENUS-PRICKLE1. After anti-GFP
537 immunoprecipitation, bound proteins were revealed with the indicated antibodies. **D.** In 293T
538 cells, PRICKLE1 was associated with RICTOR but not RAPTOR. **E.** In 293T cells, the
539 interaction between MINK1 and RICTOR is enhanced when PRICKLE1 is overexpressed. **F.**
540 In 293T cells, downregulation of PRICKLE1 leads to a decreased association between
541 MINK1 and RICTOR. **G.** Lower interaction between RICTOR and PRICKLE1 was observed
542 in the absence of MINK1. **H.** RICTOR is associated to PRICKLE1 in the presence of MINK1
543 but not MINK1-KD. **I.** In MDA-MB-231 cells, endogenous RICTOR was more associated
544 with PRICKLE1 T370D than with PRICKLE1. **J.** FLAG-MINK1 localizes at the cell cortex
545 in MDA-MB-231 cells. **K.** Colocalization of VENUS-PRICKLE1 and RICTOR at the leading
546 edge of MDA-MB-231 cells (scale bars are 20 μ M). Quantification of cortical colocalization
547 of PRICKLE1 and RICTOR and western blot analysis to confirm siRNA MINK1 efficiency
548 are provided in **L** and **M**, respectively. **N.** Model of mTORC2 recruitment at the plasma
549 membrane by PRICKLE1.

550

551 **Figure 4: Stability of focal adhesions is increased by targeting of the PRICKLE1-**
552 **mTORC2 complex.** **A.** MDA-MB-231 cells stably expressing VENUS-PAXILLIN were
553 treated with the indicated siRNAs. Top images: rainbow pictures are built by summing up and
554 assigning a different color for every time-point, from red to purple (see color-bar). Stable
555 adhesions appear in white, while dynamic adhesions appear as a pattern only partially
556 depicting the rainbow colors. Bottom images: after tracking, focal adhesion trajectories are

557 represented using the same color scheme as for encoding time. Stable adhesions, tracked over
558 the entire time-lapse movie, are circled in white, while unstable adhesions, tracked only over a
559 subset of frames, are circled in black. For each condition and in both panels, representative
560 stable and unstable adhesions are denoted by white and black arrowheads, respectively. **B.**
561 Statistical analysis representing the percentage of stable and unstable focal adhesions for each
562 siRNA treatment. **C.** Disassembly rates measured for each focal adhesion under the indicated
563 siRNA treatment. The line inside the box plot represents the median and the + sign represents
564 the mean. Student t test two tailed with 95% confidence of interval. ***P<0.001. Total
565 number (n) of focal adhesion measured is between 741 and 4156, recorded in 18 to 49
566 movies, from at least 3 independent experiments. **D.** Western blot analysis (anti-phospho-
567 PAXILLIN) of MDA-MB-231 cells treated with the indicated siRNAs. See also Figure S4.

568

569 **Figure 5: The PRICKLE1 complex phosphorylates AKT through mTORC2.** **A.** Kinetics
570 of AKT phosphorylation in MDA-MB-231 cells stimulated with 5% FCS for the indicated
571 times. **B.** and **D.** PRICKLE1 (**B**) and MINK1 (**D**) contribute to AKT phosphorylation
572 (treatment: 5% FCS during 30 min). **C.** Expression of VENUS-PRICKLE1 and VENUS-
573 PRICKLE1 potentiates AKT phosphorylation in MDA-MB-231 cells (treatment: 5% FCS
574 during 10 min). **E.** *In vitro* kinase assays were performed on anti-FLAG
575 immunoprecipitations of HEK293T cell extracts. Phosphorylation at Serine 473 of
576 recombinant AKT was evaluated by western blot. **F.** Same as **E.** Decreased expression of
577 RICTOR impaired AKT phosphorylation by the PRICKLE1 complex. **G.** Same as **B.**
578 PRICKLE1 contributes to AKT1 and AKT2 phosphorylation. **H.** AKT1 or AKT2 expression
579 was downregulated in MDA-MB-231 cells as confirmed by western blot (**J**) and focal
580 adhesion area were measured using ImageJ software. Quantification is represented in (**I**). **K.**
581 MDA-MB-231 cells seeded on collagen-coated coverslips were treated with the indicated

582 inhibitors for 16 hours. Polymerized actin was stained using phalloidin staining. Cell
583 spreading was measured and shown in **L. M.** Cells treated as in **K** were analyzed by western
584 blot using indicated antibodies. Statistical analysis was performed using one way ANOVA
585 with Tukey post-test. Statistical analysis was performed against control (black histogram).
586 **P<0.01; ***P<0.001. Data are presented as means \pm SEM. See also Figure S1, S5.

587

588 **Figure 6: Mapping of the PRICKLE1-mTORC2 complex.** **A.** Schematic of the PRICKLE1
589 mutants. **B.** Proteins extracted from HEK293T cells expressing the indicated constructs were
590 immunopurified and the presence of endogenous RICTOR was assessed. **C.** VENUS or
591 VENUS-C1 of PRICKLE1 (see **A**) were expressed in HEK293T cells and immunopurified to
592 detect the presence RICTOR. **D.** Overexpression of the C1 domain of PRICKLE was able to
593 decrease the interaction between PRICKLE1 and RICTOR. **E.** and **F.** MDA-MB-231 cells
594 were transfected with VENUS or VENUS-C1 and stimulated with FCS for 30 minutes.
595 Phosphorylation of AKT (**E**) and cell migration (**F**) were assessed by western blot and
596 Boyden chamber assays, respectively. **G** and **H.** same as (**E**) except that the transfected MDA-
597 MB-231 cells were seeded on collagen-coated coverslips. **H.** Quantification of cell spreading
598 in (**G**). Scale bar are 20 μ M. Statistical analysis was performed against control (black
599 histogram). ***P<0.001. Data are presented as means \pm SEM.

600

601

602 **Figure 7: Dominant negative effect of the C1 domain of PRICKLE1 on tumor growth**
603 **and formation of metastasis.** **A.** MDA-MB-231 cells expressing VENUS or VENUS-C1 of
604 PRICKLE1 were assayed for cell proliferation. **B.** Mice were xenografted with luciferase-
605 positive MDA-MB-231 cells expressing VENUS or VENUS-C1 of PRICKLE1. The volume
606 of primary tumors was measured after 35 days. **C-D.** Lungs (**C**) and Liver (**D**) of sacrificed

607 mice were assayed by bioluminescence. Quantification are shown in **(E)** for lungs and in **(F)**
608 for livers. **G.** Mouse tail injection of luciferase-positive MDA-MB-231. After 15 days, the
609 luminescence of the entire mouse was measured and represented in **H.** ANOVA with
610 Dunnett's correction for multiple testing was used to assess the significance of differences
611 among the different groups of animals. * $P < 0.05$; ** $P < 0.01$; *** $P < 0.001$. **I.** Box plot of
612 *PRICKLE1* expression in breast cancer cell lines. **J.** Box plot of *PRICKLE1* expression across
613 basal versus non-basal breast cancers. **K.** Kaplan-Meier curves of metastasis-free survival
614 among basal breast cancers patients according to overexpression (Up) versus no
615 overexpression (no Up) of *PRICKLE1* mRNA. **L.** Box plot of standardized protein expression
616 levels (RPPA) of the indicated proteins in TCGA breast basal cancer samples (N=85) between
617 "PRICKLE1-up" and "PRICKLE1-no up" groups. See also Figures S6 and S7, Tables S1 and
618 S2.

619 **Experimental procedures**

620 **Cell culture, transfection and antibodies**

621 HEK293T, MDA-MB-231, SKBR7, MCF7 cells were obtained from the ATCC. Cells were
622 grown in DMEM containing 10% Fetal Calf Serum. Transfections were performed using
623 Polyethyleimine (Santa Cruz), Lipofectamine 2000 and Lipofectamine LTX (Thermo). siRNA
624 were used as reverse transfection using Lipofectamine RNAimax (Thermo). Antibodies
625 targeting MINK1 and α - β 1-INTEGRIN were obtained from Bethyl. α - β 1-INTEGRIN (clone
626 9EG7) was obtained from BD Bioscience. The following antibodies were obtained from Cell
627 Signaling: α -AKT, α -pS473-AKT, α -pT308-AKT, α -RICTOR, α -mTOR, α -pS473-AKT1, α -
628 pS472-AKT2, α -pT450-AKT, α -PKC α , α -FOXO, α -pT32-FOXO, α -pY118-PAXILLIN and
629 from EMD Millipore: α -pS657-PKC α .

630 **Affinity purification, immunoprecipitation and western blot**

631 48 hours post-transfection, cells were lysed with the TAP lysis buffer and incubated at 4°C for
632 1 hour to solubilize proteins. Affinity purification and immunoprecipitations were performed
633 using either streptavidin resin (GE Healthcare) or anti-FLAG-M2 beads (Sigma) for 3 hours at
634 4°C. After extensive washes with lysis buffer, proteins were eluted with 2x Laemmli sample
635 buffer and heated at 95°C for 5 min in the presence of β -mercaptoethanol (Sigma). Whole cell
636 lysates or purified protein samples were resolved by SDS-polyacrylamide gel electrophoresis
637 (SDS-PAGE) and transferred onto Biotrace NT Nitrocellulose Transfer Membranes (Pall
638 Corporation). Western blotting were performed with antibodies as indicated in figures legend,
639 followed by chemiluminescent detection using appropriate HRP-conjugated antibodies and
640 the SuperSignal West Pico (Thermo Scientific) reagent.

641 **Boyden chamber assays**

642 50,000 cells were counted and loaded in serum starved condition in the upper chamber of a
643 Boyden chamber. Lower chamber was filled with media supplemented with 5% FCS. After 12

644 hours, migrating cells were gently recovered from the bottom side of the chamber by trypsin
645 treatment and counted using a Promega cell titer assay as described elsewhere (Puvirajesinghe
646 et al., 2016).

647 **Confocal imaging**

648 Cells were seeded on coverslips pretreated with rat tail Collagen (Roche). Cells were fixed
649 using paraformaldehyde followed by permeabilization using PBS/Triton X-100 at 0.2%. Cells
650 were treated with the indicated antibody and imaged on confocal LSM 510 META (Zeiss)
651 with a UV laser and $\times 63$ and $\times 40$ objectives. Confocal images were analyzed using ImageJ
652 software.

653 **TIRF experiments**

654 For live-cell TIRF microscopy, engineered MDA-MB-231 stably expressing venus-
655 PAXILLIN cells were siRNA transfected with the indicated siRNA and seeded 48 hours later
656 on collagen coated glass bottom Petri dishes. Cells were imaged the next day with a Roper
657 Scientific ILas2 laser illuminator for TIRF Microscopy with 491 nm laser excitation (Cobolt
658 Calyso 100 mW) on a Axio Observer Z1 microscope (ZEISS) and TIRF objective alpha plan
659 neoFluar $\times 100/1.48$ with EM-CCD Evolve 512 Camera (photometrics), and driven by
660 MetaMorph 7 software (Molecular devices).

661 ***In vitro* kinase assay**

662 The PRICKLE1 or RADIL complexes were purified from HEK293T cells stably expressing
663 FLAG-PRICKLE1 or FLAG-RADIL. Protein complexes were incubated with soluble
664 recombinant GST-AKT1 protein purified from *Escherichia coli*. Phosphorylation reactions
665 were performed in kinase buffer (25 mM Hepes, pH 7.4, 25 mM β -glycerophosphate, 25 mM
666 MgCl₂, 0.1 mM Na₃VO₄, 0.5 mM DTT) supplemented with 20 μ M ATP at 37°C for 1 hour.
667 Reactions were stopped by addition of 4x Laemmli sample buffer. Proteins were resolved by
668 SDS-PAGE and analyzed by anti-Serine 473-AKT antibody.

669

670 **Author contributions:** **A.M.D. and J.P.B.** conceived the project. **A.M.D.** designed and
671 conducted most of the experiments. **E.J.** and **R.C.** conducted animal work. **S.A.** performed
672 mass spectrometry analysis. **F.B.** and **P.F.** analyzed the clinical data. **A.S.** performed the
673 TIRF analysis. **D.B.** and **S.A.** provided expertise and feedback. **J.P.B.** supervised the project.
674 **A.M.D.** and **J.P.B.** wrote the manuscript.

675 **References**

676 Agarwal, N. K., Chen, C. H., Cho, H., Boulbes, D. R., Spooner, E., and Sarbassov, D. D. (2013).
677 Rictor regulates cell migration by suppressing RhoGDI2. *Oncogene* *32*, 2521-2526.

678 Ahmed, S. M., Theriault, B. L., Uppalapati, M., Chiu, C. W., Gallie, B. L., Sidhu, S. S., and Angers, S.
679 (2012). KIF14 negatively regulates Rap1a-Radil signaling during breast cancer progression. *J Cell*
680 *Biol* *199*, 951-967.

681 Anastas, J. N., Biechele, T. L., Robitaille, M., Muster, J., Allison, K. H., Angers, S., and Moon, R. T.
682 (2012). A protein complex of SCRIB, NOS1AP and VANGL1 regulates cell polarity and migration,
683 and is associated with breast cancer progression. *Oncogene* *31*, 3696-3708.

684 Anastas, J. N., Kulikaukas, R. M., Tamir, T., Rizos, H., Long, G. V., von Euw, E. M., Yang, P. T.,
685 Chen, H. W., Haydu, L., Toroni, R. A., *et al.* (2014). WNT5A enhances resistance of melanoma cells
686 to targeted BRAF inhibitors. *J Clin Invest* *124*, 2877-2890.

687 Belotti, E., Polanowska, J., Daulat, A. M., Audebert, S., Thome, V., Lissitzky, J. C., Lembo, F.,
688 Blibek, K., Omi, S., Lenfant, N., *et al.* (2013). The human PDZome: a gateway to PSD95-Disc large-
689 zonula occludens (PDZ)-mediated functions. *Mol Cell Proteomics* *12*, 2587-2603.

690 Burridge, K., and Chrzanowska-Wodnicka, M. (1996). Focal adhesions, contractility, and signaling.
691 *Annu Rev Cell Dev Biol* *12*, 463-518.

692 Chin, Y. R., and Toker, A. (2009). Function of Akt/PKB signaling to cell motility, invasion and the
693 tumor stroma in cancer. *Cell Signal* *21*, 470-476.

694 Ciruna, B., Jenny, A., Lee, D., Mlodzik, M., and Schier, A. F. (2006). Planar cell polarity signalling
695 couples cell division and morphogenesis during neurulation. *Nature* 439, 220-224.

696 Cordenonsi, M., Zanconato, F., Azzolin, L., Forcato, M., Rosato, A., Frasson, C., Inui, M., Montagner,
697 M., Parenti, A. R., Poletti, A., *et al.* (2011). The Hippo transducer TAZ confers cancer stem cell-
698 related traits on breast cancer cells. *Cell* 147, 759-772.

699 Cui, C., Chatterjee, B., Lozito, T. P., Zhang, Z., Francis, R. J., Yagi, H., Swanhart, L. M., Sanker, S.,
700 Francis, D., Yu, Q., *et al.* (2013). Wdpcp, a PCP protein required for ciliogenesis, regulates directional
701 cell migration and cell polarity by direct modulation of the actin cytoskeleton. *PLoS Biol* 11,
702 e1001720.

703 Daulat, A. M., Luu, O., Sing, A., Zhang, L., Wrana, J. L., McNeill, H., Winklbauer, R., and Angers, S.
704 (2012). Mink1 regulates beta-catenin-independent Wnt signaling via Prickle phosphorylation. *Mol*
705 *Cell Biol* 32, 173-185.

706 Dissanayake, S. K., Wade, M., Johnson, C. E., O'Connell, M. P., Leotlela, P. D., French, A. D., Shah,
707 K. V., Hewitt, K. J., Rosenthal, D. T., Indig, F. E., *et al.* (2007). The Wnt5A/protein kinase C pathway
708 mediates motility in melanoma cells via the inhibition of metastasis suppressors and initiation of an
709 epithelial to mesenchymal transition. *J Biol Chem* 282, 17259-17271.

710 Dow, L. E., Elsum, I. A., King, C. L., Kinross, K. M., Richardson, H. E., and Humbert, P. O. (2008).
711 Loss of human Scribble cooperates with H-Ras to promote cell invasion through deregulation of
712 MAPK signalling. *Oncogene* 27, 5988-6001.

713 Escobedo, N., Contreras, O., Munoz, R., Farias, M., Carrasco, H., Hill, C., Tran, U., Pryor, S. E.,
714 Wessely, O., Copp, A. J., and Larrain, J. (2013). Syndecan 4 interacts genetically with Vangl2 to
715 regulate neural tube closure and planar cell polarity. *Development* 140, 3008-3017.

716 Facchinetti, V., Ouyang, W., Wei, H., Soto, N., Lazorchak, A., Gould, C., Lowry, C., Newton, A. C.,
717 Mao, Y., Miao, R. Q., *et al.* (2008). The mammalian target of rapamycin complex 2 controls folding
718 and stability of Akt and protein kinase C. *EMBO J* 27, 1932-1943.

719 Gubb, D., and Garcia-Bellido, A. (1982). A genetic analysis of the determination of cuticular polarity
720 during development in *Drosophila melanogaster*. *J Embryol Exp Morphol* 68, 37-57.

721 Gujral, T. S., Chan, M., Peshkin, L., Sorger, P. K., Kirschner, M. W., and MacBeath, G. (2014). A
722 noncanonical Frizzled2 pathway regulates epithelial-mesenchymal transition and metastasis. *Cell* *159*,
723 844-856.

724 Gulhati, P., Bowen, K. A., Liu, J., Stevens, P. D., Rychahou, P. G., Chen, M., Lee, E. Y., Weiss, H. L.,
725 O'Connor, K. L., Gao, T., and Evers, B. M. (2011). mTORC1 and mTORC2 regulate EMT, motility,
726 and metastasis of colorectal cancer via RhoA and Rac1 signaling pathways. *Cancer Res* *71*, 3246-
727 3256.

728 Houalla, T., Hien Vuong, D., Ruan, W., Suter, B., and Rao, Y. (2005). The Ste20-like kinase
729 misshapen functions together with Bicaudal-D and dynein in driving nuclear migration in the
730 developing drosophila eye. *Mech Dev* *122*, 97-108.

731 Hu, Y., Leo, C., Yu, S., Huang, B. C., Wang, H., Shen, M., Luo, Y., Daniel-Issakani, S., Payan, D. G.,
732 and Xu, X. (2004). Identification and functional characterization of a novel human misshapen/Nck
733 interacting kinase-related kinase, hMINK beta. *J Biol Chem* *279*, 54387-54397.

734 Jacinto, E., Loewith, R., Schmidt, A., Lin, S., Ruegg, M. A., Hall, A., and Hall, M. N. (2004).
735 Mammalian TOR complex 2 controls the actin cytoskeleton and is rapamycin insensitive. *Nat Cell*
736 *Biol* *6*, 1122-1128.

737 Jenny, A., Darken, R. S., Wilson, P. A., and Mlodzik, M. (2003). Prickle and Strabismus form a
738 functional complex to generate a correct axis during planar cell polarity signaling. *EMBO J* *22*, 4409-
739 4420.

740 Kim, E. K., Yun, S. J., Ha, J. M., Kim, Y. W., Jin, I. H., Yun, J., Shin, H. K., Song, S. H., Kim, J. H.,
741 Lee, J. S., *et al.* (2011). Selective activation of Akt1 by mammalian target of rapamycin complex 2
742 regulates cancer cell migration, invasion, and metastasis. *Oncogene* *30*, 2954-2963.

743 Lamouille, S., Connolly, E., Smyth, J. W., Akhurst, R. J., and Derynck, R. (2012). TGF-beta-induced
744 activation of mTOR complex 2 drives epithelial-mesenchymal transition and cell invasion. *J Cell Sci*
745 *125*, 1259-1273.

746 Lewellyn, L., Cetera, M., and Horne-Badovinac, S. (2013). Misshapen decreases integrin levels to
747 promote epithelial motility and planar polarity in *Drosophila*. *J Cell Biol* *200*, 721-729.

748 Luga, V., Zhang, L., Vitoria-Petit, A. M., Ogunjimi, A. A., Inanlou, M. R., Chiu, E., Buchanan, M.,
749 Hosein, A. N., Basik, M., and Wrana, J. L. (2012). Exosomes mediate stromal mobilization of
750 autocrine Wnt-PCP signaling in breast cancer cell migration. *Cell* *151*, 1542-1556.

751 MacGrath, S. M., and Koleske, A. J. (2012). Cortactin in cell migration and cancer at a glance. *J Cell*
752 *Sci* *125*, 1621-1626.

753 Matsuda, Y., Schlange, T., Oakeley, E. J., Boulay, A., and Hynes, N. E. (2009). WNT signaling
754 enhances breast cancer cell motility and blockade of the WNT pathway by sFRP1 suppresses MDA-
755 MB-231 xenograft growth. *Breast Cancer Res* *11*, R32.

756 Matsumoto, S., Fumoto, K., Okamoto, T., Kaibuchi, K., and Kikuchi, A. (2010). Binding of APC and
757 dishevelled mediates Wnt5a-regulated focal adhesion dynamics in migrating cells. *EMBO J* *29*, 1192-
758 1204.

759 McDonald, P. C., Oloumi, A., Mills, J., Dobрева, I., Maidan, M., Gray, V., Wederell, E. D., Bally, M.
760 B., Foster, L. J., and Dedhar, S. (2008). Rictor and integrin-linked kinase interact and regulate Akt
761 phosphorylation and cancer cell survival. *Cancer Res* *68*, 1618-1624.

762 Munoz, R., Moreno, M., Oliva, C., Orbenes, C., and Larrain, J. (2006). Syndecan-4 regulates non-
763 canonical Wnt signalling and is essential for convergent and extension movements in *Xenopus*
764 embryos. *Nat Cell Biol* *8*, 492-500.

765 Narimatsu, M., Bose, R., Pye, M., Zhang, L., Miller, B., Ching, P., Sakuma, R., Luga, V., Roncari, L.,
766 Attisano, L., and Wrana, J. L. (2009). Regulation of planar cell polarity by Smurf ubiquitin ligases.
767 *Cell* *137*, 295-307.

768 Parsons, J. T., Horwitz, A. R., and Schwartz, M. A. (2010). Cell adhesion: integrating cytoskeletal
769 dynamics and cellular tension. *Nat Rev Mol Cell Biol* *11*, 633-643.

770 Partovian, C., Ju, R., Zhuang, Z. W., Martin, K. A., and Simons, M. (2008). Syndecan-4 regulates
771 subcellular localization of mTOR Complex2 and Akt activation in a PKCalpha-dependent manner in
772 endothelial cells. *Mol Cell* *32*, 140-149.

773 Pearson, H. B., Perez-Mancera, P. A., Dow, L. E., Ryan, A., Tennstedt, P., Bogani, D., Elsum, I.,
774 Greenfield, A., Tuveson, D. A., Simon, R., and Humbert, P. O. (2011). SCRIB expression is

775 deregulated in human prostate cancer, and its deficiency in mice promotes prostate neoplasia. *J Clin*
776 *Invest* 121, 4257-4267.

777 Perou, C. M., Sorlie, T., Eisen, M. B., van de Rijn, M., Jeffrey, S. S., Rees, C. A., Pollack, J. R., Ross,
778 D. T., Johnsen, H., Akslen, L. A., *et al.* (2000). Molecular portraits of human breast tumours. *Nature*
779 406, 747-752.

780 Pukrop, T., Klemm, F., Hagemann, T., Gradl, D., Schulz, M., Siemes, S., Trumper, L., and Binder, C.
781 (2006). Wnt 5a signaling is critical for macrophage-induced invasion of breast cancer cell lines. *Proc*
782 *Natl Acad Sci U S A* 103, 5454-5459.

783 Puvirajesinghe, T. M., Bertucci, F., Jain, A., Scerbo, P., Belotti, E., Audebert, S., Sebbagh, M., Lopez,
784 M., Brech, A., Finetti, P., *et al.* (2016). Identification of p62/SQSTM1 as a component of non-
785 canonical Wnt VANGL2-JNK signalling in breast cancer. *Nat Commun* 7, 10318.

786 Salles, A., Billaudeau, C., Serge, A., Bernard, A. M., Phelipot, M. C., Bertaux, N., Fallet, M., Grenot,
787 P., Marguet, D., He, H. T., and Hamon, Y. (2013). Barcoding T cell calcium response diversity with
788 methods for automated and accurate analysis of cell signals (MAAACS). *PLoS Comput Biol* 9,
789 e1003245.

790 Saoncella, S., Echtermeyer, F., Denhez, F., Nowlen, J. K., Mosher, D. F., Robinson, S. D., Hynes, R.
791 O., and Goetinck, P. F. (1999). Syndecan-4 signals cooperatively with integrins in a Rho-dependent
792 manner in the assembly of focal adhesions and actin stress fibers. *Proc Natl Acad Sci U S A* 96, 2805-
793 2810.

794 Sarbassov, D. D., Ali, S. M., Kim, D. H., Guertin, D. A., Latek, R. R., Erdjument-Bromage, H.,
795 Tempst, P., and Sabatini, D. M. (2004). Rictor, a novel binding partner of mTOR, defines a
796 rapamycin-insensitive and raptor-independent pathway that regulates the cytoskeleton. *Curr Biol* 14,
797 1296-1302.

798 Sarbassov, D. D., Guertin, D. A., Ali, S. M., and Sabatini, D. M. (2005). Phosphorylation and
799 regulation of Akt/PKB by the rictor-mTOR complex. *Science* 307, 1098-1101.

800 Schaller, M. D., and Parsons, J. T. (1995). pp125FAK-dependent tyrosine phosphorylation of paxillin
801 creates a high-affinity binding site for Crk. *Mol Cell Biol* 15, 2635-2645.

802 Sorlie, T., Perou, C. M., Tibshirani, R., Aas, T., Geisler, S., Johnsen, H., Hastie, T., Eisen, M. B., van
803 de Rijn, M., Jeffrey, S. S., *et al.* (2001). Gene expression patterns of breast carcinomas distinguish
804 tumor subclasses with clinical implications. *Proc Natl Acad Sci U S A* 98, 10869-10874.

805 Takeuchi, M., Nakabayashi, J., Sakaguchi, T., Yamamoto, T. S., Takahashi, H., Takeda, H., and Ueno,
806 N. (2003). The prickle-related gene in vertebrates is essential for gastrulation cell movements. *Curr*
807 *Biol* 13, 674-679.

808 Tao, H., Suzuki, M., Kiyonari, H., Abe, T., Sasaoka, T., and Ueno, N. (2009). Mouse prick1, the
809 homolog of a PCP gene, is essential for epiblast apical-basal polarity. *Proc Natl Acad Sci U S A* 106,
810 14426-14431.

811 Tao, J. J., Castel, P., Radosevic-Robin, N., Elkabets, M., Auricchio, N., Aceto, N., Weitsman, G.,
812 Barber, P., Vojnovic, B., Ellis, H., *et al.* (2014). Antagonism of EGFR and HER3 enhances the
813 response to inhibitors of the PI3K-Akt pathway in triple-negative breast cancer. *Sci Signal* 7, ra29.

814 Tomar, A., Lawson, C., Ghassemian, M., and Schlaepfer, D. D. (2012). Cortactin as a target for FAK
815 in the regulation of focal adhesion dynamics. *PLoS One* 7, e44041.

816 Veeman, M. T., Slusarski, D. C., Kaykas, A., Louie, S. H., and Moon, R. T. (2003). Zebrafish prick1,
817 a modulator of noncanonical Wnt/Fz signaling, regulates gastrulation movements. *Curr Biol* 13, 680-
818 685.

819 von Maltzahn, J., Bentzinger, C. F., and Rudnicki, M. A. (2012). Wnt7a-Fzd7 signalling directly
820 activates the Akt/mTOR anabolic growth pathway in skeletal muscle. *Nat Cell Biol* 14, 186-191.

821 Wei, W., Li, H., Li, N., Sun, H., Li, Q., and Shen, X. (2013). WNT5A/JNK signaling regulates
822 pancreatic cancer cells migration by Phosphorylating Paxillin. *Pancreatology* 13, 384-392.

823 Wu, X., Renuse, S., Sahasrabudhe, N. A., Zahari, M. S., Chaerkady, R., Kim, M. S., Nirujogi, R. S.,
824 Mohseni, M., Kumar, P., Raju, R., *et al.* (2014). Activation of diverse signalling pathways by
825 oncogenic PIK3CA mutations. *Nat Commun* 5, 4961.

826 Yunokawa, M., Koizumi, F., Kitamura, Y., Katanasaka, Y., Okamoto, N., Kodaira, M., Yonemori, K.,
827 Shimizu, C., Ando, M., Masutomi, K., *et al.* (2012). Efficacy of everolimus, a novel mTOR inhibitor,
828 against basal-like triple-negative breast cancer cells. *Cancer Sci* 103, 1665-1671.

829 Zallen, J. A. (2007). Planar polarity and tissue morphogenesis. *Cell* 129, 1051-1063.

830 Zhang, F., Zhang, X., Li, M., Chen, P., Zhang, B., Guo, H., Cao, W., Wei, X., Cao, X., Hao, X., and
831 Zhang, N. (2010). mTOR complex component Rictor interacts with PKCzeta and regulates cancer cell
832 metastasis. *Cancer Res* *70*, 9360-9370.

833 Zoncu, R., Efeyan, A., and Sabatini, D. M. (2011). mTOR: from growth signal integration to cancer,
834 diabetes and ageing. *Nat Rev Mol Cell Biol* *12*, 21-35.

835

836

FIGURE 1

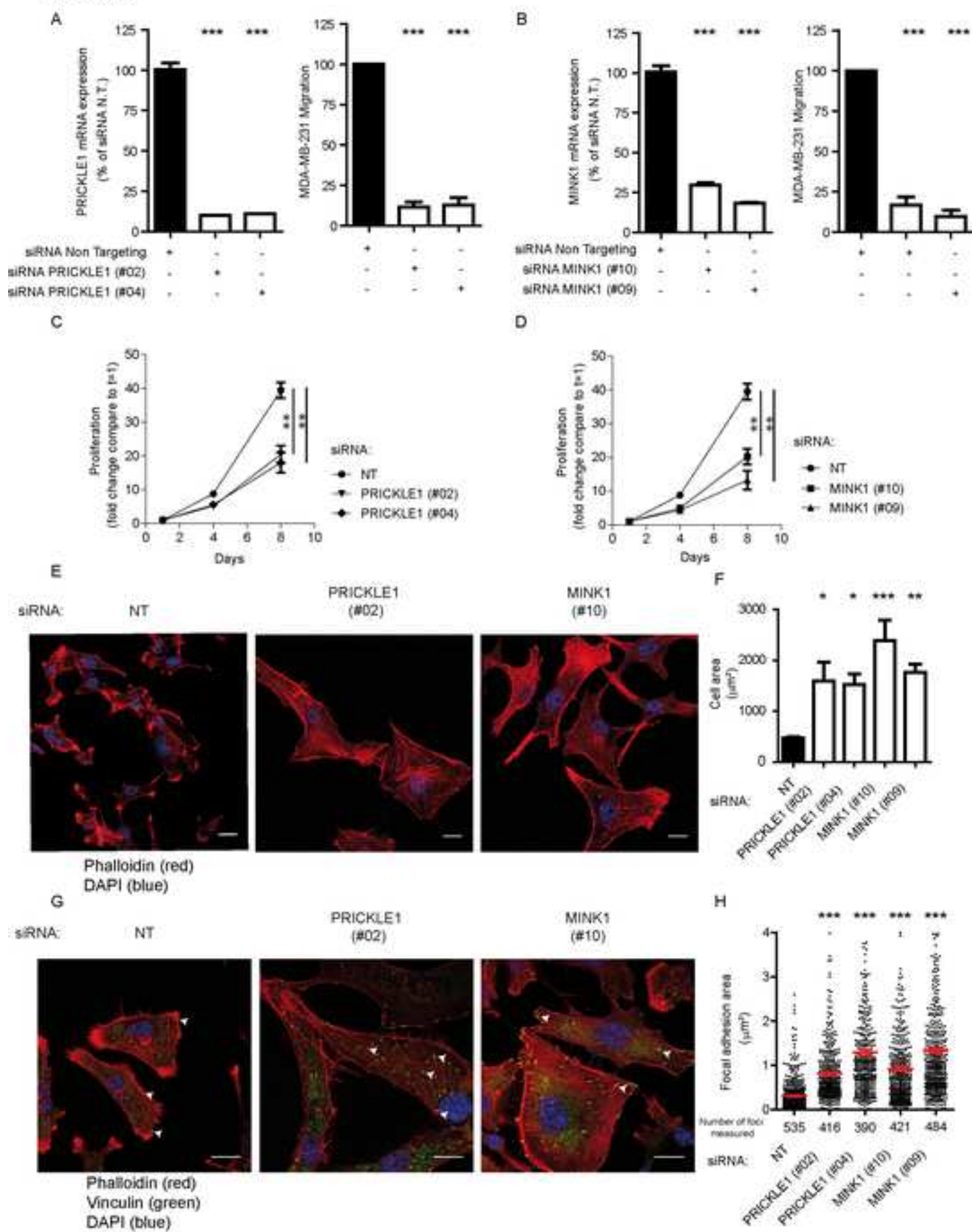


FIGURE 2

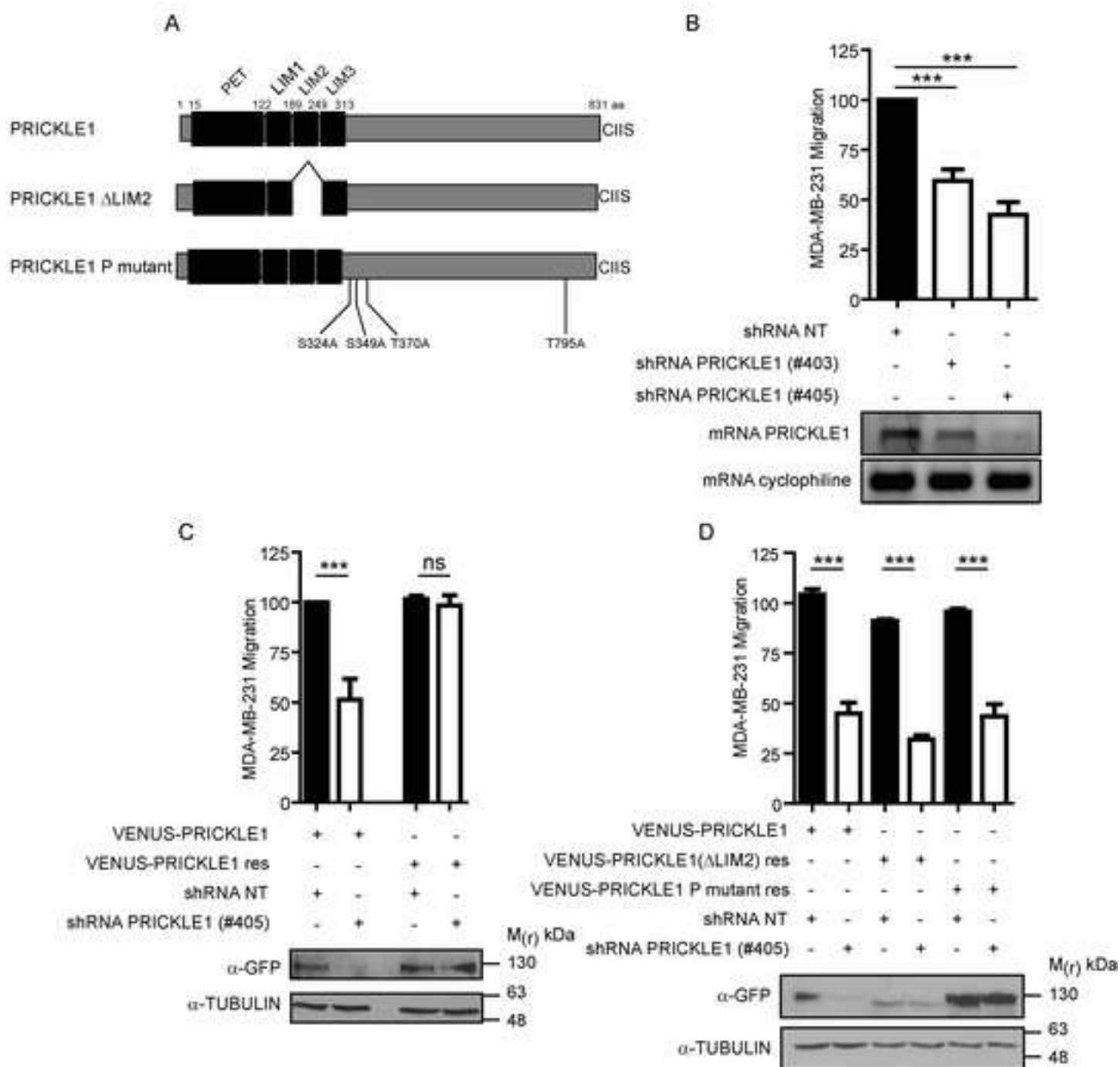


FIGURE 3

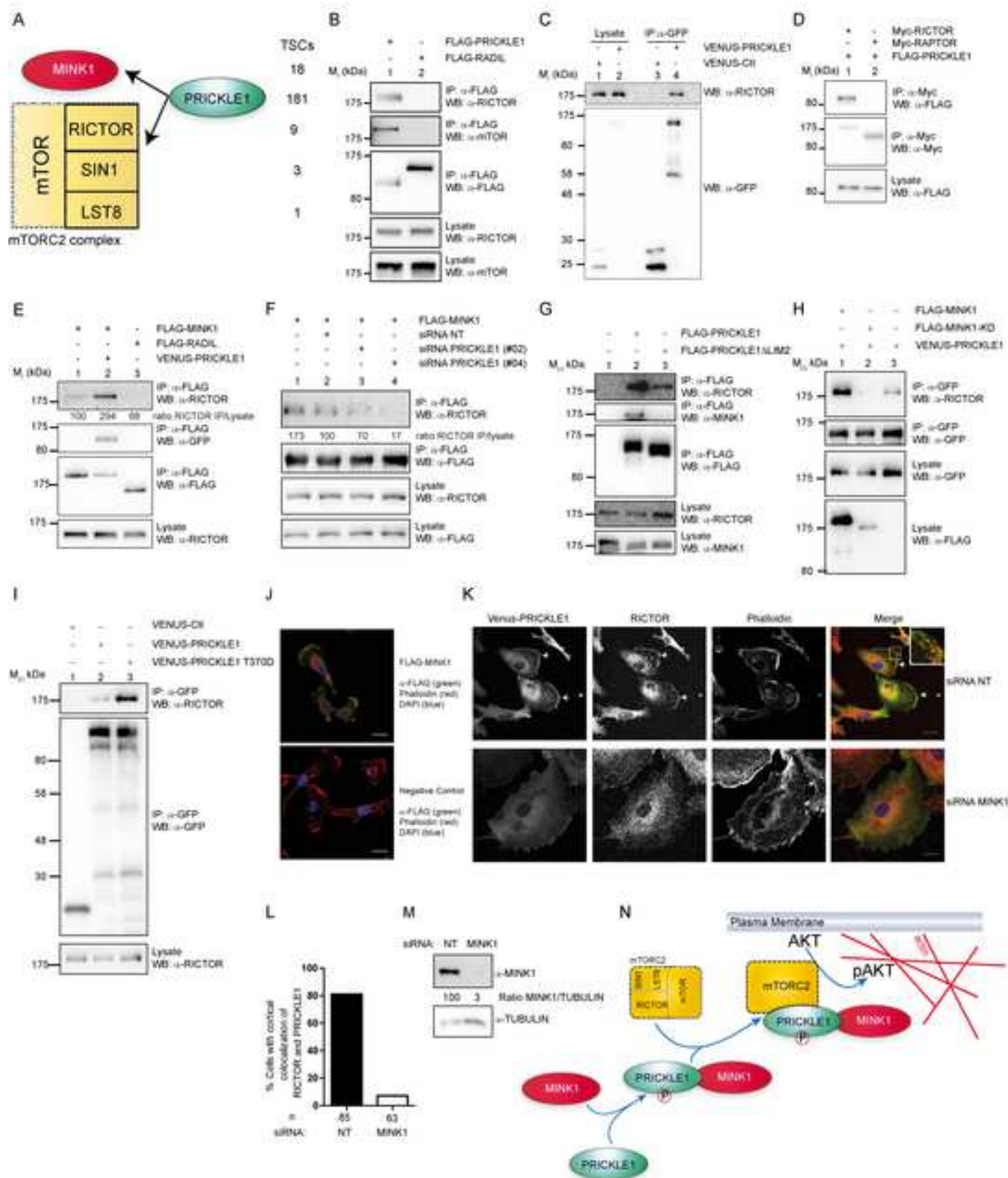


FIGURE 4

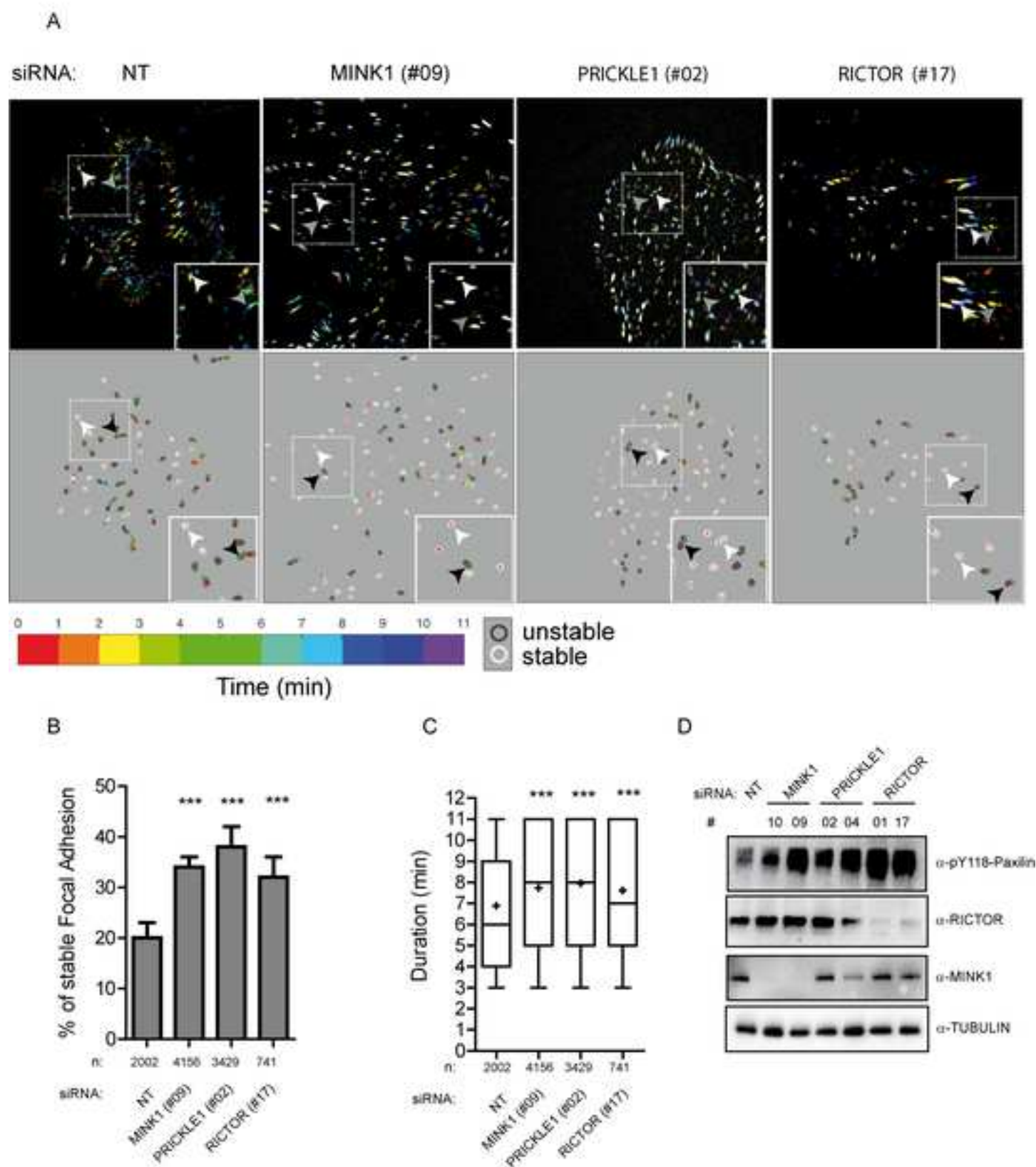


FIGURE 5

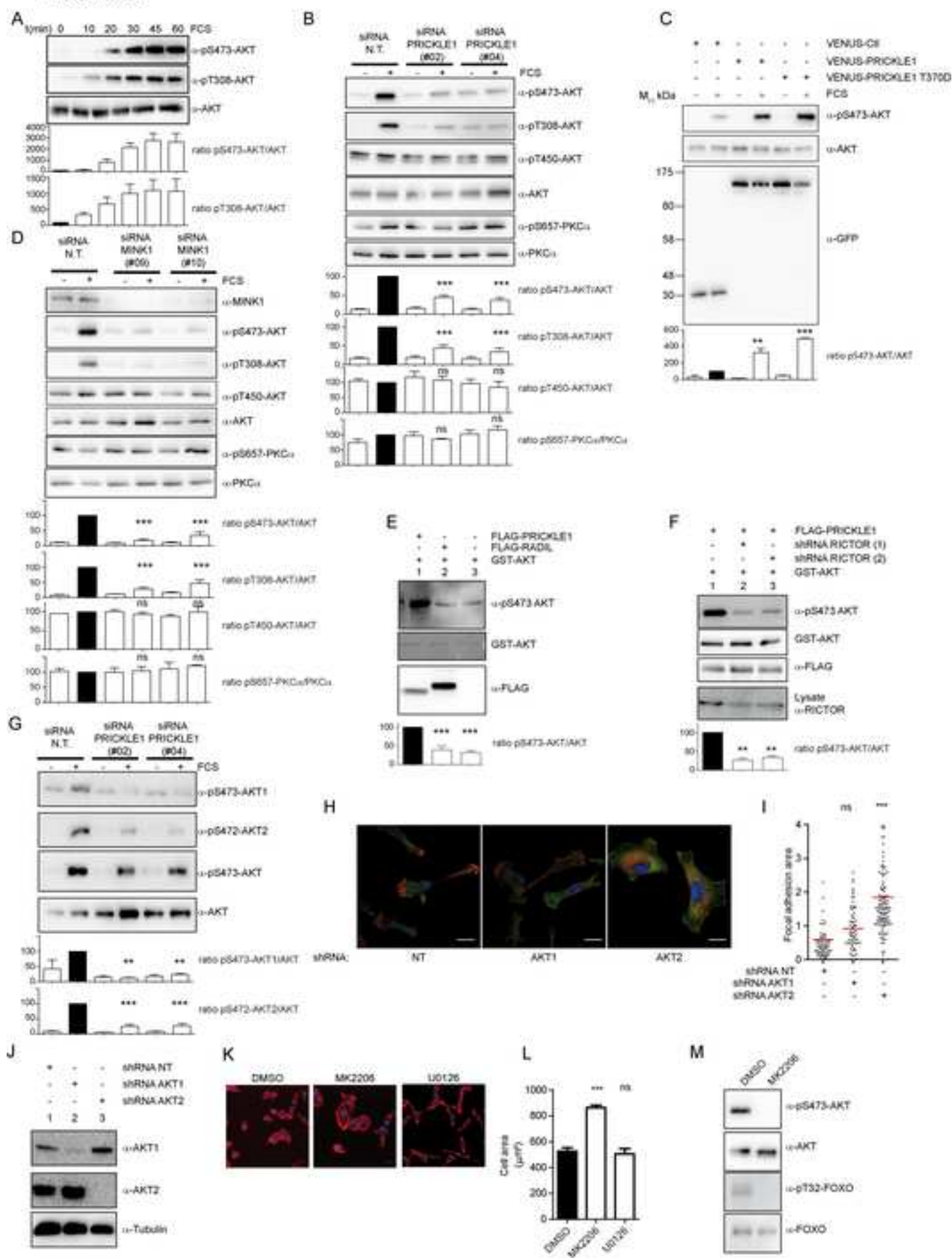


FIGURE 6

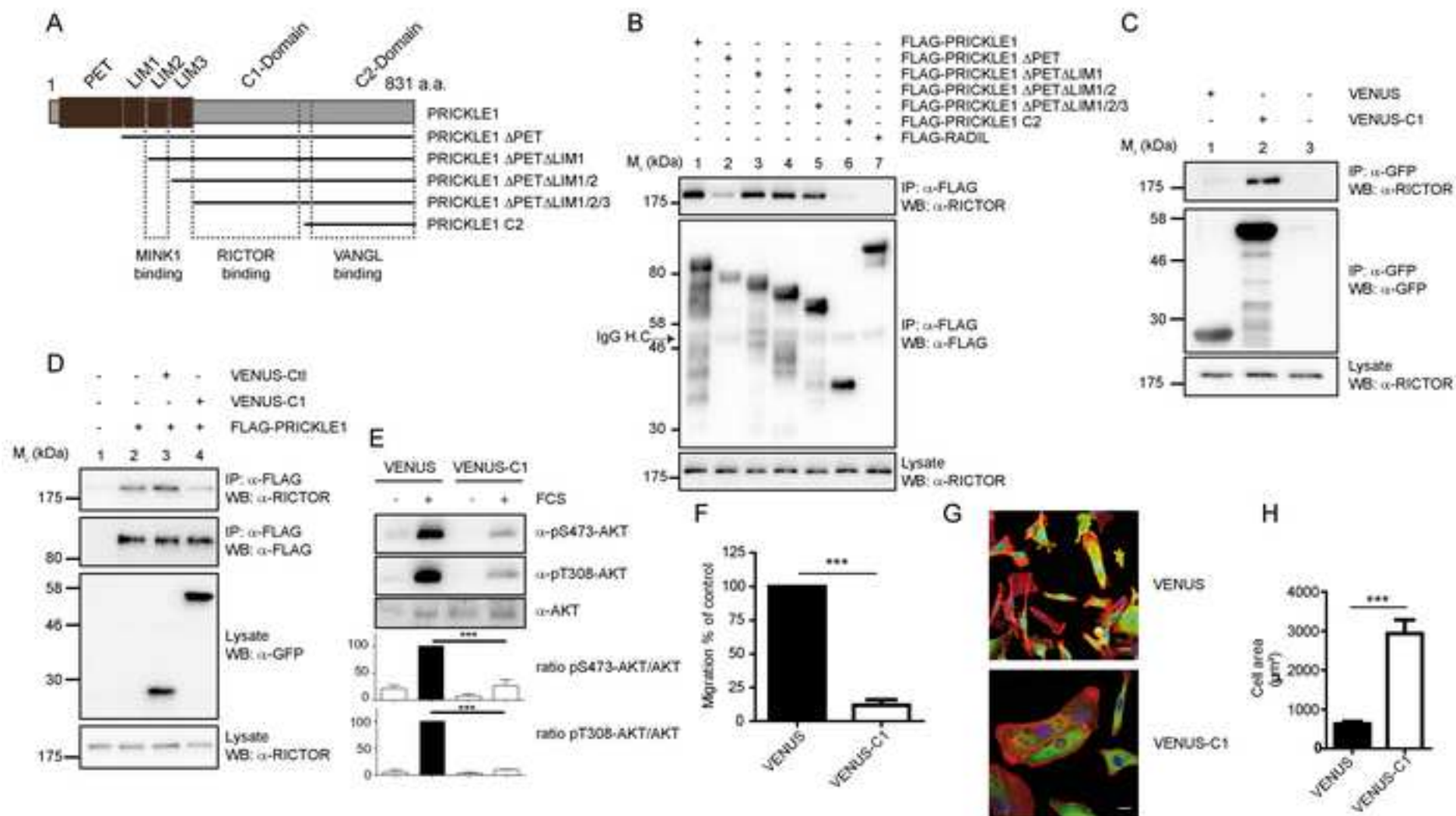
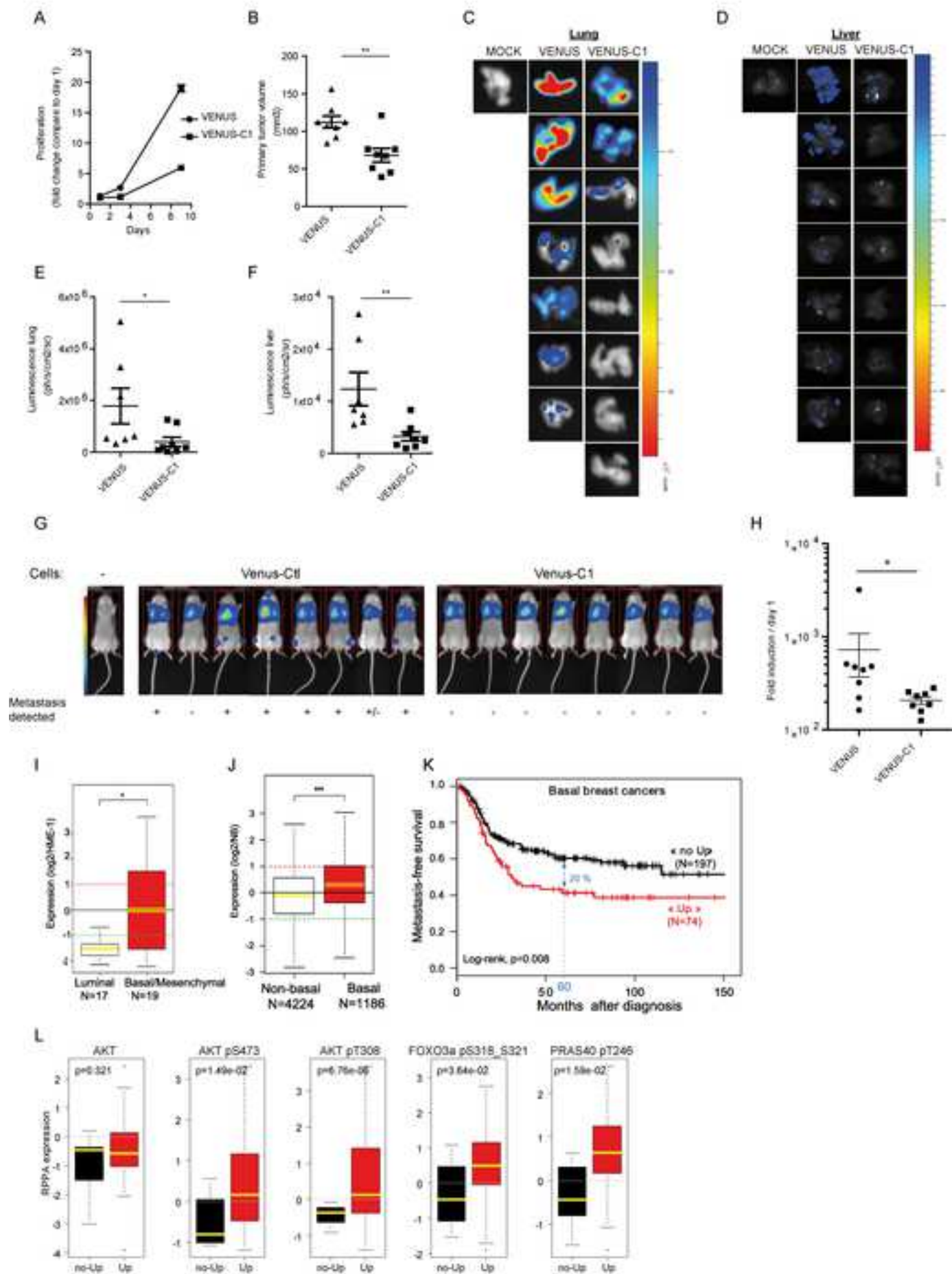


FIGURE 7



Supplemental Information

PRICKLE1 contributes to cancer cell dissemination
through its interaction with mTORC2

Avais M. Daulat, François Bertucci, Stéphane Audebert, Arnaud Sergé, Pascal Finetti,
Emmanuelle Josselin, Rémy Castellano, Daniel Birnbaum, Stéphane Angers, and Jean-Paul
Borg

FIGURE S1 related to Fig. 1, 5 and 6: Actin cytoskeleton remodelling in MDA-MB-231 cells.

FIGURE S2 related to Fig. 1: PRICKLE1 and MINK1 are required for cytoskeleton
organization and cell migration.

FIGURE S3 related to Fig. 1: β -integrin activity and internalization is controlled by the
MINK1-PRICKLE1-RICTOR protein complex.

FIGURE S4, related to Fig. 4: RICTOR is involved in cell migration and cell proliferation of
MDA-MB-231 cells.

FIGURE S5, related to Fig. 5: PRICKLE1 regulates AKT phosphorylation in SKBR7 cells.

FIGURE S6, related to Fig. 7: MINK1 plays a role in tumor growth and cancer cell
dissemination.

FIGURE S7, related to Fig. 7: Overexpression of PRICKLE1 mRNA in basal breast cancer,
correlation with poor prognosis and AKT phosphorylation.

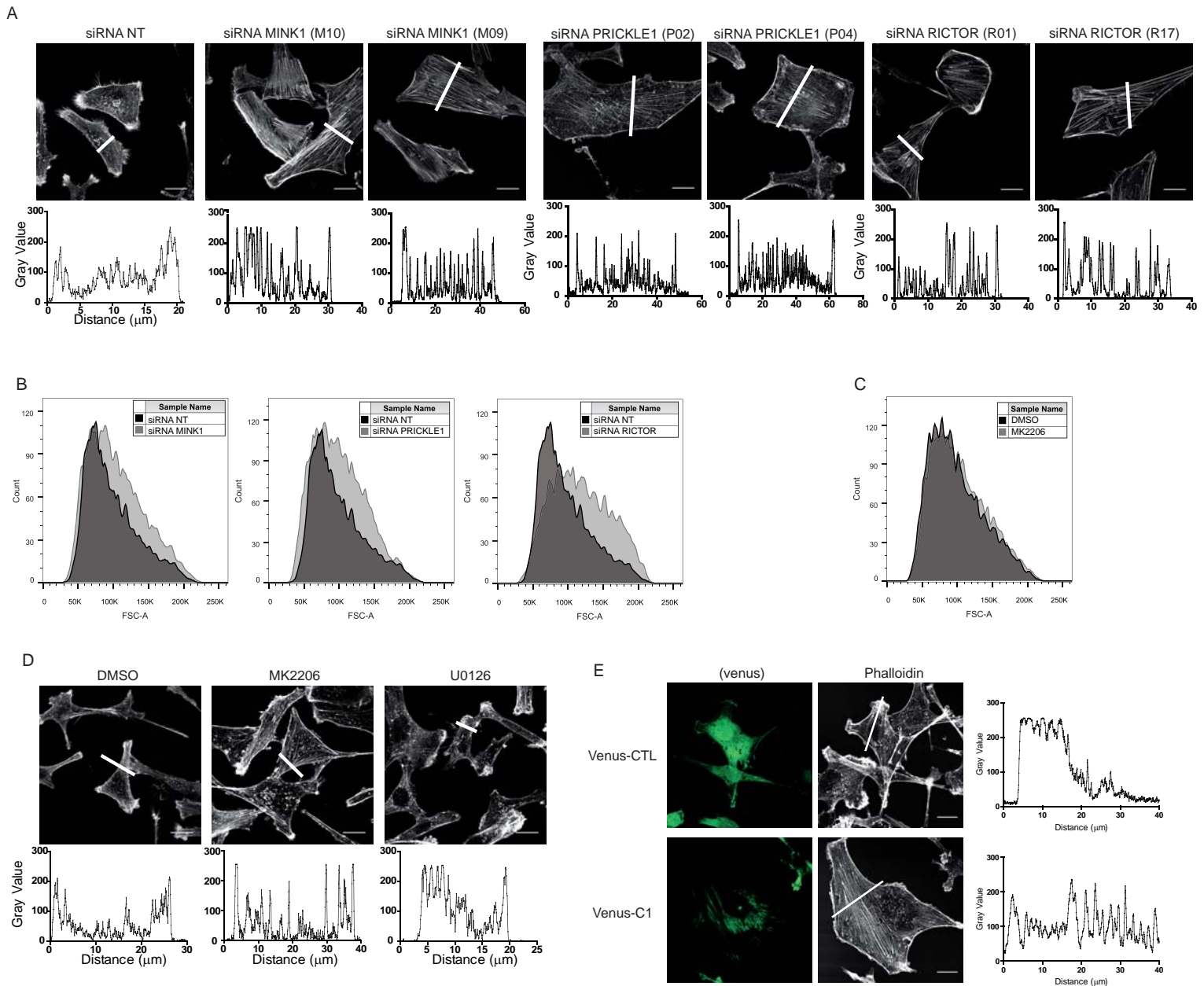
Supplementary Table 1 related to Fig. 7 and S7: List of breast cancer data sets included in the
gene expression analysis and *PRICKLE1* expression-based groups.

Supplementary Table 2 related to Fig. 7 and S7: Clinicopathological characteristic of patients
and samples included in the gene expression analysis

Supplementary Material and Methods

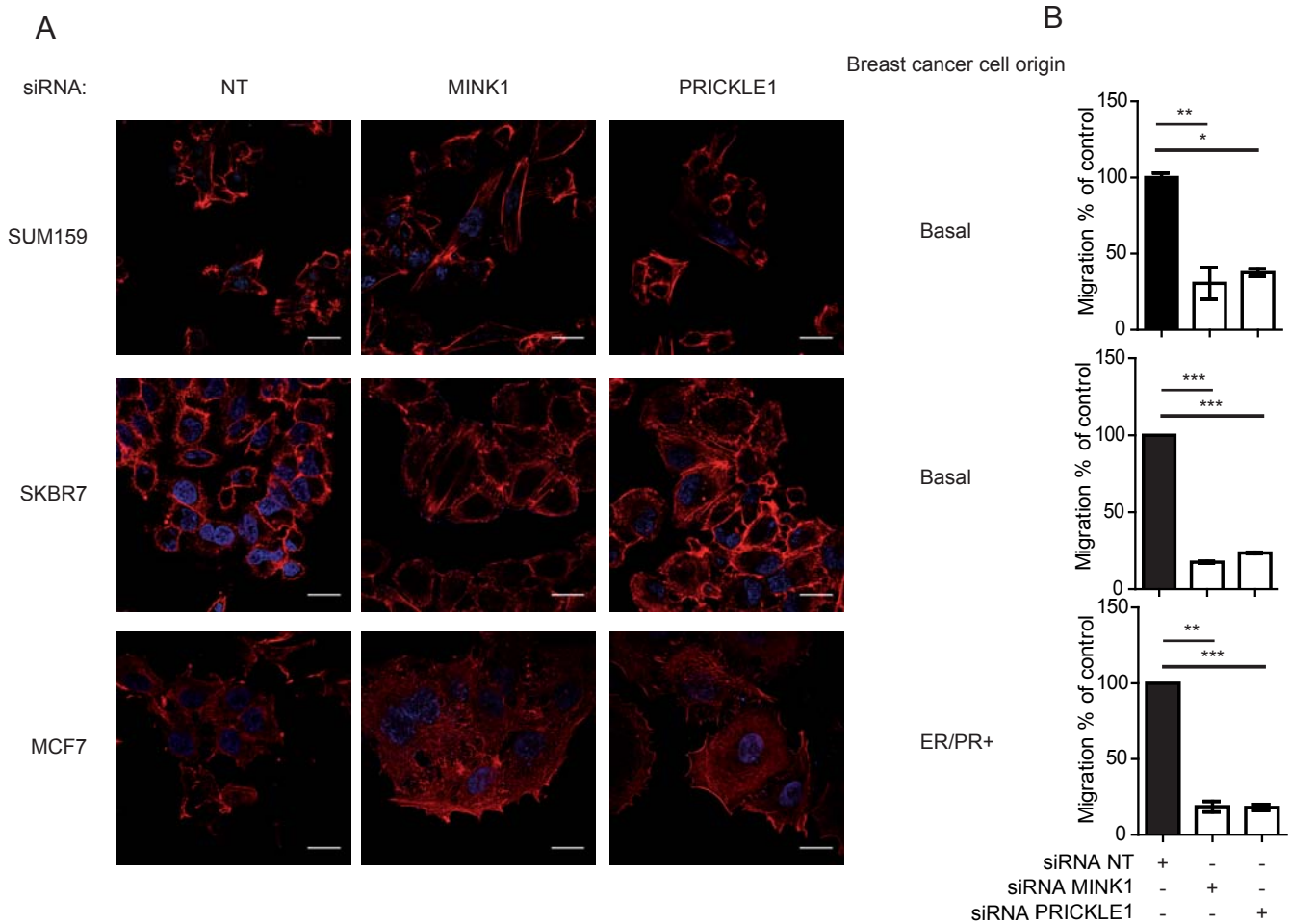
Supplementary References

FIGURE S1 related to Fig. 1, 5 and 6



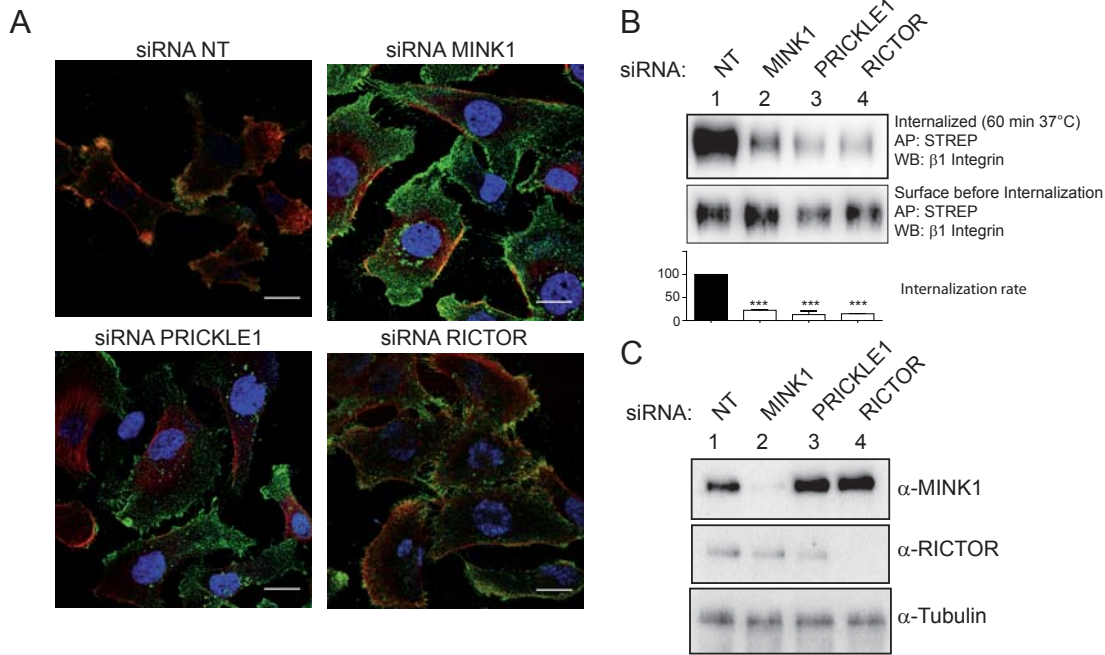
Actin cytoskeleton remodelling in MDA-MB-231 cells. A. Confocal images of F-actin in cells treated as indicated and following spreading for 24 hours on collagen coated coverslips ($n=3$). A line was drawn and the intensity profile plotted (below) to show the relative distribution of actin bundles in cells. **B-C.** Flow cytometry analysis based on forward scatter (FSC-A) to measure the relative cell size under downregulation of PRICKLE1, MINK1 or RICTOR compare to control cells (siRNA NT) (**B**) or MK2206 treatment (**C**). **D.** Inhibition of AKT and mTORC2 alters actin cytoskeleton. Confocal images of F-actin in cells treated as indicated. Cells were first seeded for 24 hours on collagen coated coverslips and treated for 16 hours with the indicated drugs ($n=3$). Cells were treated as follows: MK2206 ($1\mu\text{M}$) and U0126 ($1\mu\text{M}$). A line was drawn and the intensity profile plotted (below) to show the relative distribution of actin bundles in cells. **E.** Expression of VENUS-C1 leads to cytoskeleton reorganization. Confocal images of F-actin in cells treated as indicated following spreading on collagen coated coverslips for 24 hours ($n=3$). A line was drawn and the intensity profile plotted (below) to show the relative distribution of actin bundles in cells.

FIGURE S2 related to Fig. 1



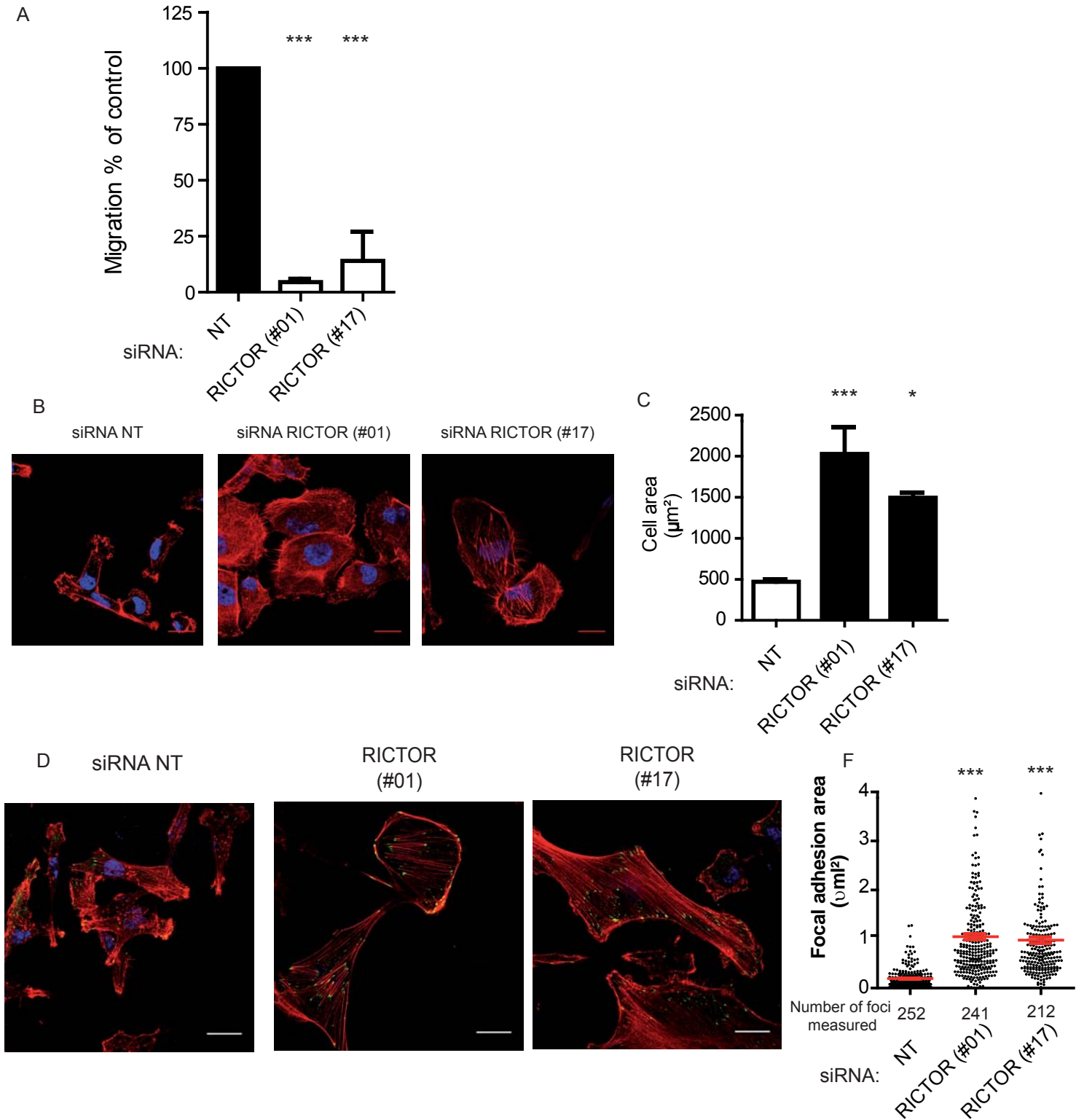
PRICKLE1 and MINK1 are required for cytoskeleton organization and cell migration. **A.** siRNAs directed against PRICKLE1 or MINK1 were transfected into SUM159, SKBR7 and MCF7 cells and seeded on collagen-coated cover slips. After fixation, cells were stained with Phalloidin (red) to reveal polymerized actin and DAPI (blue). Scale bars are 20 μ M. Images are representative of three independent experiments. **B.** Migration assays using Boyden chamber assays show that downregulation of either PRICKLE1 or MINK1 leads to a decrease of cell motility.

FIGURE S3 related to Fig. 1



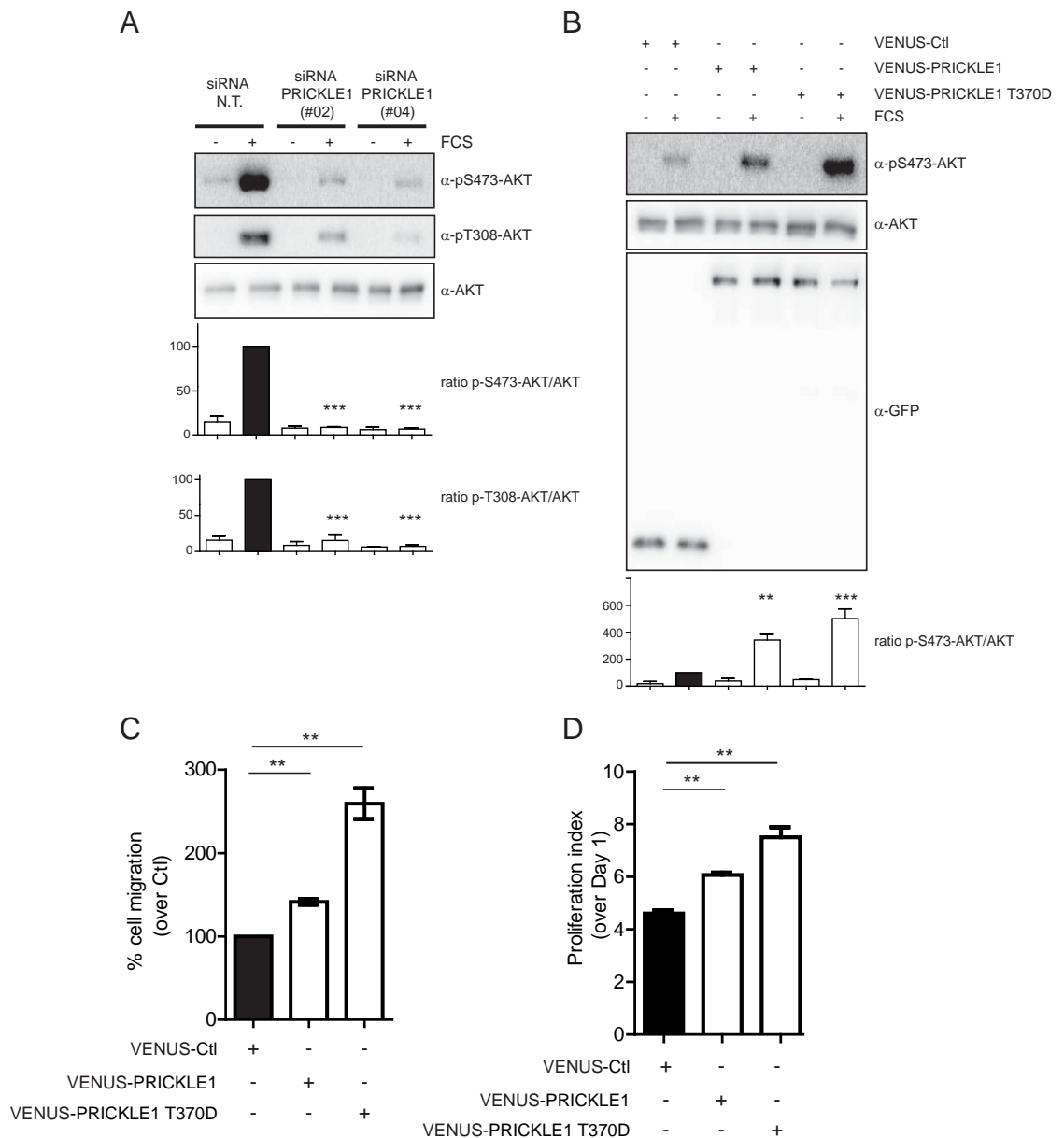
β 1-integrin activity and internalization is controlled by the MINK1-PRICKLE1-RICTOR protein complex. **A.** MDA-MB-231 cells were treated with the indicated siRNAs and seeded on collagen coated coverslips. After fixation with PFA, cells were stained with anti- β 1-integrin (clone 9EG7) shown in green. Actin is shown in red and nucleus was stained with DAPI (blue). After acquisition, we observed an increase of activated β 1-integrin staining under MINK1, PRICKLE1 and RICTOR downregulation. We also observed that staining was not restricted within the lamellipodium as observed with siRNA NT condition but all over the surface of the cells. **B.** Internalization assay was performed using surface labelling with biotin followed by streptavidin pull down. We observed after 60 min of FCS treatment that cells downregulated for MINK1, PRICKLE1 and RICTOR have a decrease of β 1-integrin internalization. **C.** Western blot analysis to confirm downregulation efficiency of the indicated siRNA treatment. Western blot quantification is presented in the inset. Statistical analysis was performed using on way ANOVA with Turkey post-test. **P<0.01 and ***P<0.001.

FIGURE S4, related to Fig. 4



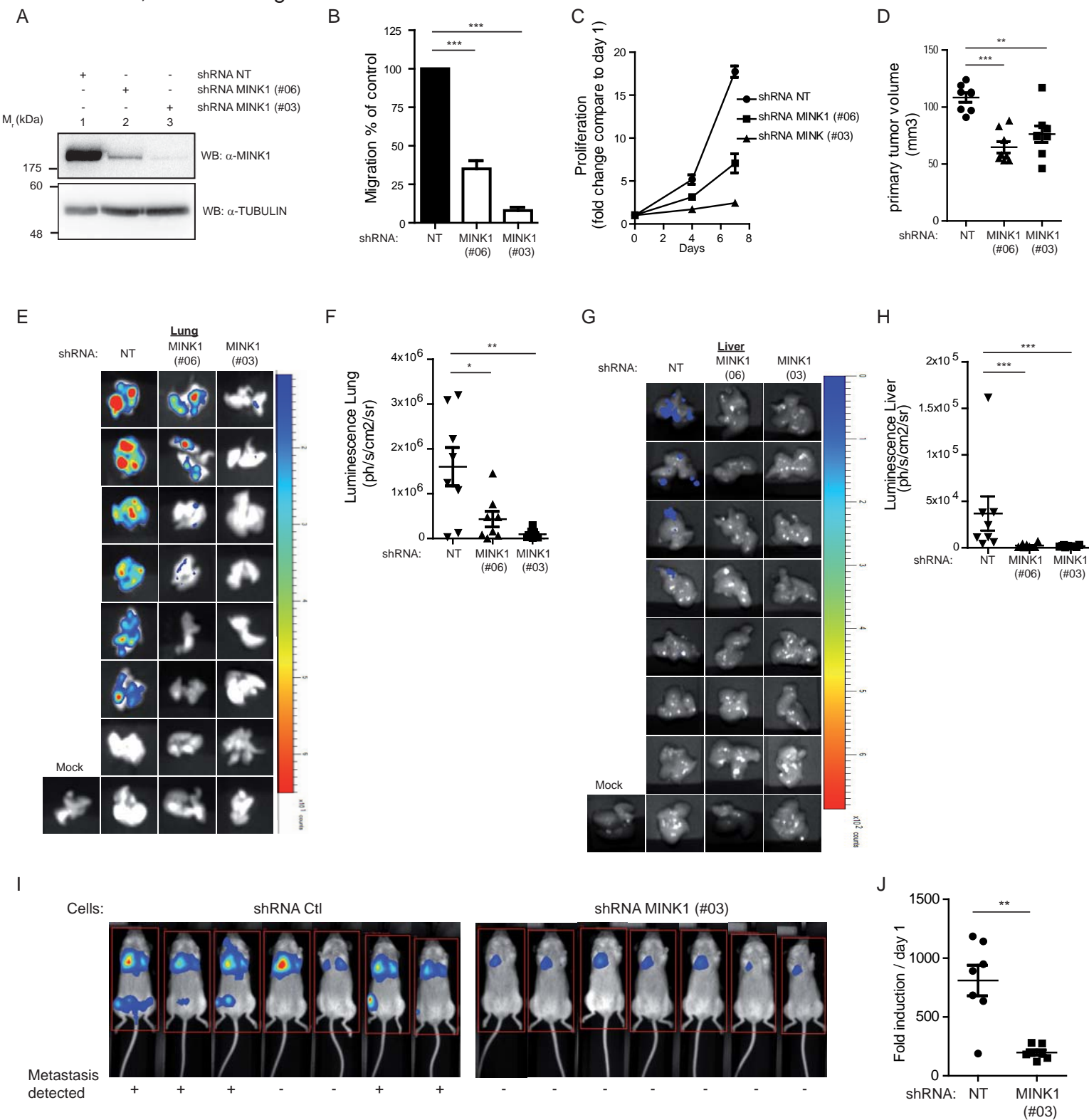
RICTOR is involved in cell migration and cell proliferation of MDA-MB-231 cells. **A.** Inhibition of RICTOR expression decreases MDA-MB-231 cell motility. Two independent siRNAs targeting RICTOR or a control siRNA (Non Targeting, NT) were transfected into MDA-MB-231 cells. Loss of RICTOR mRNA expression was confirmed by western blot (data not shown). Transfected cells were subjected to a cell migration assay using Boyden chambers. **B.** Two independent siRNAs directed against RICTOR were transfected into MDA-MB-231 cells seeded on collagen-coated cover slips. After fixation, cells were stained with Phalloidin (red) to reveal polymerized actin and DAPI (blue). Scale bars are 20μm. Images are representative of three independent experiments. **C.** Statistical analysis of experiments presented in (B). Cell areas were measured using ImageJ software. Statistical analysis was performed using one way ANOVA with Tukey post-test. *P <0.05; ***P<0.001. **D.** Same as (B) except that staining was done performed with phalloidin (red), α-Vinculin antibody (green) and DAPI (blue). Images are representative of three independent experiments. Scale bars are 20 μm. **E.** Sizes of focal adhesions were measured using vinculin staining and ImageJ software analysis. Data represent the statistical repartition spread of focal adhesion area when RICTOR is downregulated by two independent siRNAs

FIGURE S5, related to Fig. 5



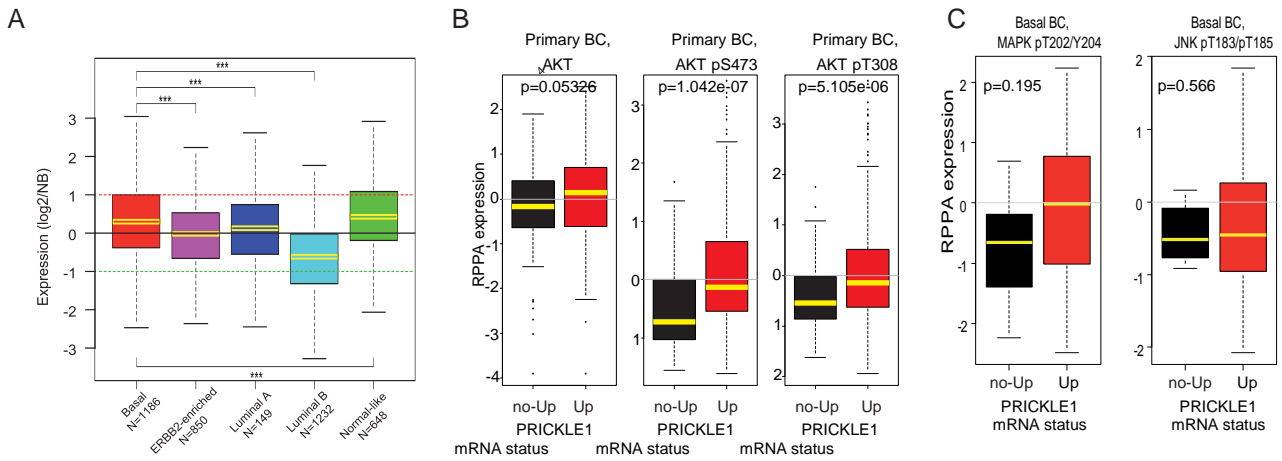
PRICKLE1 regulates AKT phosphorylation in SKBR7 cells. **A.** SKBR7 cells were subjected to downregulation of PRICKLE1 expression using siRNA treatment. Cells were serum starved during 16 hours before being stimulated with 5%FCS during 30 min. PRICKLE1 downregulation leads to a decrease of AKT activation after FCS stimulation at Serine 473 and Threonine 308. **B.** Overexpression of VENUS-PRICKLE1 and VENUS-PRICKLE1 T370D increases AKT activation under FCS stimulation. Fold induction is given by measuring the ratio between pS473-AKT and total AKT. **C-D.** SKBR7 expressing VENUS-PRICKLE1 or VENUS-PRICKLE1 T370D have higher cell migration in boyden chamber assays as shown in C, and higher proliferation as shown in D. Western blot quantification is presented in the inset. Statistical analysis was performed using on way ANOVA with Turkey post-test. **P<0.01 and ***P<0.001.

FIGURE S6, related to Fig. 7



MINK1 plays a role in tumor growth and cancer cell dissemination. **A.** Western blot analysis using anti-MINK1 antibody of MDA-MB-231 cells stably expressing either a non-targeting shRNA (shRNA NT) or two shRNAs targeting MINK1 expression. **B.** MDA-MB-231 cells subjected to stable downregulation of MINK1 were assayed in Boyden chamber assays: downregulation of MINK1 was associated with a decrease of cell proliferation. **C.** MDA-MB-231 cells subjected to stable downregulation of MINK1 were evaluated in cell proliferation assays: downregulation of MINK1 was associated with a decrease of cell proliferation. **D.** Luciferase-positive MDA-MB-231 cells stably expressing shRNAs were xenografted into the fat pads of SCID mice. After 35 days, the volume of primary tumors was measured: downregulation of MINK1 was associated with a decrease of tumor volume. **E.** Images of the lungs from sacrificed mice obtained by bioluminescence. Before sacrifice, an intraperitoneal injection of luciferine allowed the detection of MDA-MB-231 cells present in the lung. In the cohort of mice injected with MDA-MB-231 cells, 6 out of 8 had lungs colonized by MDA-MB-231 cells. Mice injected with MDA-MB-231 cells stably expressing shRNA MINK1 (#06) or (#03) developed lung metastasis in 4 (out of 6) mice and 1 (out of 6) mice, respectively. Total luminescence was measured in the lung and reported in **F**. **G.** The same investigation for liver metastasis in the cohort of mice injected with MDA-MB-231 cells, 4 out of 8 had liver colonized by MDA-MB-231 cells. Mice injected with MDA-MB-231 cells stably expressing shRNA MINK1 (#06) or (#03) do not developed liver metastasis, quantification in **H**. **I.** Tail vein injection of luciferase positive MDA-MB-231 cells stably downregulating for MINK1 expression. Images were taken after 21 days and show luminescence in the lungs in both conditions and within the rear part of the mouse in control condition only. Quantification of the fold induction of luciferase between days 1 to 21 were given in **J**. ANOVA with Dunnett's correction for multiple testing was used to assess the significance of differences among the different groups of animals. * $p < 0.05$; ** $p < 0.01$; *** $p < 0.001$.

FIGURE S7, related to Fig. 7



Overexpression of PRICKLE1 mRNA in basal breast cancer, correlation with poor prognosis and AKT phosphorylation. A. Box plot of PRICKLE1 expression across 5,410 patient samples. Difference in expression levels between breast cancer subtypes classified as basal, ERBB2-enriched, luminal A, luminal B, and normal-like. The data show an increased expression of PRICKLE1 mRNA in basal breast cancers. *P<0.05; ***P<0.001. **B.** Boxplot of standardized protein expression levels (RPPA) of AKT and 2 phosphorylated forms (i.e. pS473 and pT308) in TCGA breast cancer samples (N=368) between “PRICKLE1-up” group and “PRICKLE1-no up”. **C.** Boxplot of standardized protein expression levels (RPPA) of phosphorylated forms of MAPK (pT202/Y204) and JNK (pT183/pT185) in TCGA breast basal cancer samples (N=85) between “PRICKLE1-up” group and “PRICKLE1-no up”.

Supplementary Table 1 related to Fig. 7 and S7: List of breast cancer data sets included in the gene expression analysis

Reference	Source of data	N° of samples analyzed*	Technological platform	N° of probe sets
Ivshina et al., Cancer Res 2006	GEO database GSE4922_1456	448	Affymetrix U133 A+B	2x22K
Bonnefoi et al., Lancet Oncol 2007	GEO database GSE6861/GSE4779	125	Affymetrix X3P	22K
Guedj et al., Oncogene 2012	Array Express, E-MTAB-365	452	Affymetrix U133 Plus 2.0	54K
Desmedt et al., J Clin Oncol 2011	GEO database GSE16446	120	Affymetrix U133 Plus 2.0	54K
Korde et al., Breast Cancer Res Treat 2010	GEO database GSE18728	61	Affymetrix U133 Plus 2.0	54K
Expression Project in Oncology	GEO database GSE2109	348	Affymetrix U133 Plus 2.0	54K
Hoeflich et al., Clin Cancer Res 2009	GEO database GSE12763	30	Affymetrix U133 Plus 2.0	54K
Marty et al., Breast Cancer Res 2008	GEO database GSE13787	23	Affymetrix U133 Plus 2.0	54K
Bos et al., Nature 2009	GEO database GSE12276	204	Affymetrix U133 Plus 2.0	54K
Barry et al., J Clin Oncol 2010	GEO database GSE23593	50	Affymetrix U133 Plus 2.0	54K
Silver et al., J Clin Oncol 2010	GEO database GSE18864	84	Affymetrix U133 Plus 2.0	54K
Chen et al., Breast Cancer Res Treat 2010	GEO database GSE10780	42	Affymetrix U133 Plus 2.0	54K
Sabatier et al., PLoS ONE 2011	GEO database GSE 31448	352	Affymetrix U133 Plus 2.0	54K
Jönsson et al., Breast Cancer Research 2010	GEO database GSE22133	344	SWEGENE H_v2.1.1	55K
The Cancer Genome Atlas Network, Nature 2012	TCGA Data Portal (https://tcga-data.nci.nih.gov/tcga/)	534	Agilent custom 244K	244K
Ellis et al., Nature 2012	GEO database GSE35191	201	Agilent-014850 Whole Human Genome Microarray 4x44K G4112F	4x44K
Curtis et al., Nature 2012	EGA database EGAS00000000083	1992	Illumina HT 12	48K

* only non redundant primary tumors are included in the analyses

Supplementary Table 2 related to Fig. 7 and S7: Clinicopathological characteristic of patients and samples included in the gene expression analysis and *PRICKLE1* expression-based groups

Characteristics	All BCs	PRICKLE1 expression-based group		P .value
		no up	up	
Age (years)				8,61E-08
<=50	1244 (28%)	987 (26%)	257 (36%)	
>50	3207 (72%)	2756 (74%)	451 (64%)	
Pathological tumor size, pT				0,197
pT1	1244 (44%)	1042 (39%)	202 (43%)	
pT2	1592 (51%)	1371 (52%)	221 (47%)	
pT3	276 (9%)	232 (9%)	44 (9%)	
Pathological axillary lymph node status, pN				4,95E-02
negative	1937 (50%)	1643 (50%)	294 (46%)	
positive	1971 (50%)	1625 (50%)	346 (54%)	
Pathological type				1,83E-05
ductal	2913 (81%)	2479 (82%)	434 (76%)	
lobular	276 (8%)	204 (7%)	72 (13%)	
mixt	120 (3%)	98 (3%)	22 (4%)	
other	277 (8%)	237 (8%)	40 (7%)	
SBR grade				6,66E-03
1	465 (21%)	368 (10%)	97 (14%)	
2	1759 (42%)	1478 (42%)	281 (42%)	
3	1989 (47%)	1693 (48%)	296 (44%)	
ER status				2,70E-17
negative	1647 (30%)	1280 (28%)	367 (43%)	
positive	3763 (70%)	3270 (72%)	493 (57%)	
PR status				2,68E-04
negative	2566 (48%)	2108 (47%)	458 (54%)	
positive	2789 (52%)	2394 (53%)	395 (46%)	
ERBB2 status				9,31E-03
negative	4719 (87%)	3945 (87%)	774 (90%)	
positive	691 (13%)	605 (13%)	86 (10%)	
Molecular subtypes				1,00E-06
Basal	1186 (22%)	885 (19%)	301 (35%)	
ERBB2-enriched	850 (16%)	756 (17%)	94 (11%)	
Luminal A	1494 (28%)	1245 (27%)	249 (29%)	
Luminal B	1232 (23%)	1194 (26%)	38 (4%)	
Normal-like	648 (12%)	470 (10%)	178 (21%)	
5-year metastasis-free survival [CI95]	61% [58-65]	61% [58-65]	63% [56-69]	0,487

Supplementary Material and Methods

DNA constructs, siRNAs and shRNAs

The following sequences of siRNA were used to target MINK1 (#9) GGAACAAACUGCGGGUGUA, MINK1 (#10) GAAGUGGUCUAAGAAGUUC, PRICKLE1 (#02) GAGAGAAGCAUCGGAUUA, PRICKLE1 (#04) GAAGAUAAAUGGAGGUGAA, RICTOR (#1) UCAACGAGCUCACAUUGA, RICTOR (#17) GCAGAUGAGUCUUACGGAA. shRNAs were cloned into PLKO backbone and lentiviral particles were produced using PSPAX and VSV-G systems in HEK293T cells. The following sequences of shRNA were used to target MINK1 (#03) AGCGGCTCAAGGTCATCTATG, MINK1 (#06) GCTACTGAAGTTTCCCTTCAT, PRICKLE1 (#403) GCTCAGCATGTGACGAGATAA, PRICKLE1 (#405) CCACCACATGATAATGAGGTA, AKT1 GAGTTTGAGTACCTGAAGCTG and AKT2 GCGTGGTGAATACATCAAGAC. Lentiviral vectors coding for shRNAs targeting RICTOR were obtained from Addgene (plasmids #1854 and #1853). The PSL9-VENUS-PAXILLIN construct was described elsewhere (Ahmed et al., 2012). AKT1 cDNA was cloned in the PGEX4 vector to generate a recombinant GST protein. Myc-RICTOR and myc-RAPTOR were obtained from Addgene (plasmids #11367 and #1859, respectively).

β 1-integrin internalization assay

MDA-MB-231 cells were treated with siRNAs directed against Ctl, MINK1, PRICKLE1 or RICTOR in 6-wells dishes. After 48 h, cells were washed three times with PBS supplemented with 2mM MgCl₂ and biotinylated for 20 min with reducible sulfo-NHS-SS-biotin (Pierce) at 4°C. After stimulation with FCS 10% for 1 hour at 37°C, cell surface biotin was removed by treatment (2x20 min) at 4°C with sodium 2-mercaptoethanesulphonate (MesNa, Sigma). To

determine the intracellular pools of biotinylated integrin, cells were lysed and incubated with streptavidin resin (Thermo Scientific). After capture and washes, the complexes were separated by SDS-PAGE and β 1-integrin was detected by western blot. Signals were detected by chemiluminescence.

Immunopurification

5×10^7 HEK293T cells expressing either FLAG-PRICKLE1 were used for affinity purification procedure. Briefly, cells were lysed and solubilized in TAP lysis buffer (0.1% Igepal CA 630, 10% glycerol, 50mM Hepes-NaOH; pH 8.0, 150mM NaCl, 2mM EDTA, 2mM DTT, 10mM NaF, 0.25mM NaOVO₃, 50mM β -glycerophosphate, and protease inhibitor cocktail (Calbiochem). After 30 min centrifugation at 40,000xg (18,000 rpm in a Beckman JA20 rotor), the soluble fraction is incubated overnight at 4°C with anti-FLAG M2 beads (Sigma). Beads were washed with TAP lysis buffer followed by 50mM ammonium bicarbonate. Finally, proteins were eluted twice from the beads using 200 μ l of 500mM ammonium hydroxide at pH 11.0. The eluted fraction was evaporated by speedvac and the remaining pellet was then washed with 100 μ l of milliQ water. The pellet was then resuspended in 50mM ammonium bicarbonate, reduced with 25mM DTT and alkylated with 100mM iodoacetamide (Sigma) and supplemented with 1mM CaCl₂ (Bioshop) prior to digestion with 1 μ g of sequencing-grade trypsin (Promega).

Mass spectrometry analysis

Mass spectrometry analysis was carried out by LC-MSMS using a LTQ-Velos-Orbitrap (Thermo Electron, Bremen, Germany) online with a nanoLC Ultimate 3000 chromatography system (Dionex, Sunnyvale, CA). 5 μ l corresponding to 1/5th of whole sample were injected on the system. After pre-concentration and washing of the sample on a Dionex Acclaim PepMap 100 C18 column (2cm \times 100 μ m i.d. 100 A, 5 μ m particle size), peptides were separated on a Dionex Acclaim PepMap RSLC C18 column (15cm \times 75 μ m i.d., 100 A, 2 μ m

particle size) at a flow rate of 300nL/min a two steps linear gradient (4-20% acetonitrile/H₂O; 0.1 % formic acid for 90 min and 20-45-45% acetonitrile/H₂O; 0.1 % formic acid for 30 min. The separation of the peptides was monitored by a UV detector (absorption at 214 nm). For peptides ionization in the nanospray source, spray voltage was set at 1.4 kV and the capillary temperature at 275°C. All samples were measured in a data dependent acquisition mode. Each run was preceded by a blank MS run in order to monitor system background. Peptide masses are measured in a survey full scan (scan range 300-1700 m/z, with 30 K FWHM resolution at m/z=400, target AGC value of 1.00×10⁶ and maximum injection time of 500 ms). In parallel to the high-resolution full scan in the Orbitrap, the data-dependent CID scans of the 10 most intense precursor ions were fragmented and measured in the linear ion trap (normalized collision energy of 35 %, activation time of 10 ms, target AGC value of 1.00×10⁴, maximum injection time 100 ms, isolation window 2 Da). Parent masses obtained in orbitrap analyzer were automatically calibrated on 445.1200 locked mass. The fragment ion masses are measured in the linear ion trap to have a maximum sensitivity and the maximum amount of MS/MS data. Dynamic exclusion was implemented with a repeat count of 1 and exclusion duration of 30 s. Raw files generated from mass spectrometry analysis were processed with Proteome Discoverer 1.4 (ThermoFisher Scientific). This software was used to search data via in-house Mascot server (version 2.4.1; Matrix Science Inc., London, UK) against the Human subset (20,194 sequences) of the SwissProt database (version 2014_10). Database search were performed using the following settings: a maximum of two trypsin miscleavage allowed, methionine oxidation, N-terminal protein acetylation as variable modifications, cysteine carbamido-methylation as fixed modification. A peptide mass tolerance of 6 ppm and a fragment mass tolerance of 0.8 Da were used for search analysis. Only peptides with high stringency Mascot score threshold (identity, FDR<1%) were used for protein identification. The mass spectrometry proteomics data have been deposited to the ProteomeXchange

Consortium via the PRIDE (Vizcaino et al., 2016) partner repository with the dataset identifier PXD003784.

Cell size measurement

Cells were incubated with the indicated siRNAs for 48 hours or MK2206 at 1 μ M for 16 hours and then treated with trypsin-EDTA and fixed with 2% PFA. Data acquisition was performed on a LSR2® flow cytometer (BD Biosciences) and analyzed using FlowJo Software (Tree Star).

Quantitative RT-PCR

mRNA were extracted using kit supplier protocol (PROMEGA) and RT-PCR was performed as described previously (Ahmed et al., 2012). PRICKLE1 forward primer

TGCTGCCTTGAGTGTGAAAC, PRICKLE1 reverse primer

CACAAGAAAAGCAGGCTTCC. MINK1 forward primer ATCATGAACGTGCCTGGAG,

MINK1 reverse primer TCCTTCTGCTCCTCTATGCG.

Mouse experiments

NOD/SCID (non-obese diabetic/severe combined immunodeficient)/gc null mice (NSG)) were obtained from Charles River Laboratory Charles River France or bred in-house and maintained under specific pathogen-free conditions. 5x10⁵ Luciferase-expressing MDA-MB-231 cells were transplanted (100 μ L PBS 1x/matrigel, vol/vol) into mammary fat pads of mice (6-8 week-old female). For tail vein injections, luciferase-expressing MDA-MB-231 cells (0.5 \times 10⁶ cells suspended in 100 μ L of PBS) were inoculated in the tail vein of NSG mice. After completion of the analysis, autopsy of mice was done, the tumors were weighted and organ luminescence was assessed. Bioluminescence analysis was performed using PhotonIMAGER (BiospaceLab), following intraperitoneal injection of luciferin (30 mg/kg).

***PRICKLE1* mRNA expression analysis in breast cancer samples**

We analyzed the mRNA expression of *PRICKLE1* in mammary cell lines by exploring our previously published gene expression data of 45 cell lines profiled using oligonucleotide microarrays (Charafe-Jauffret et al., 2006): BT-20, BT-474, BT-483, CAMA-1, HBL100, HCC38, HCC202, HCC1395, HCC1500, HCC1569, HCC1806, HCC1937, HCC1954, HME-1, carcinosarcoma-derived Hs578T, MCF-7, MCF-10A, MDA-MB-134, MDA-MB-157, MDA-MB-175, MDA-MB-231, MDA-MB-361, MDA-MB-415, MDA-MB-436, MDA-MB-453, SK-BR-3, SK-BR-7, T47D, UACC-812, ZR-75-1, ZR-75-30 (<http://www.atcc.org/>), HMEC-derived 184A1 and 184B5 (ATCC, <http://www.atcc.org/>), BrCa-MZ-01, SUM44, SUM-52, SUM102, SUM-149, SUM159, SUM-185, SUM-190, SUM206, SUM-225, SUM229 (http://www.cancer.med.umich.edu/breast_cell/production), and S68 (a kind gift from V. Catros, Cell Biology Department, CHU Rennes, France). All cell lines are derived from carcinomas except MCF-10A, which is derived from a fibrocystic disease, and HME-1 and 184B5, which represent normal mammary tissue. The molecular subtypes (luminal, basal, and mesenchymal) were defined as previously reported (Ross and Perou, 2001). Seventeen cell lines were classified as luminal, 19 as basal or mesenchymal, whereas 9 could not be classified in any subtype.

PRICKLE1 mRNA expression in breast cancer and normal breast was analyzed in our own gene expression dataset (352 patients with invasive adenocarcinoma and 4 pools of normal breast (NB) tissue samples (11 healthy women) (Sabatier et al., 2011) coupled with publicly available data sets. The 16 public data sets comprising at least one probe set representing *PRICKLE1* were collected from the National Center for Biotechnology Information (NCBI)/Genbank GEO database, the European Bioinformatics Institute (EBI) ArrayExpress database or at the authors' websites (**Supplementary Table 1**). This resulted in a total of 5,410 non-redundant pre-therapeutic samples of non-metastatic, non-inflammatory, primary, invasive breast cancers with *PRICKLE1* mRNA expression and clinicopathological

annotations (**Supplementary Table 2**). Data analysis required pre-analytic processing. For the non-Affymetrix-based data sets, we applied quantile normalization to available processed data. Regarding the Affymetrix-based data sets, we used Robust Multichip Average (RMA) (Irizarry et al., 2003) with the non-parametric quartile algorithm as normalization parameter. Then, hybridization probes were mapped across the different technological platforms represented as previously described (Bertucci et al., 2015). To be comparable across data sets and to exclude bias from population heterogeneity, *PRICKLE1* expression levels were standardized within each data set using the luminal A population as reference. All steps were done in R using Bioconductor and associated packages. Expression level for each tumor was then centered by the average expression level of the 4 NB samples. *PRICKLE1* upregulation in a tumor was defined by a ratio tumor/NB ≥ 2 , the other cases being defined as “no upregulation”. The molecular subtypes of tumors were defined using the PAM50 predictor (Parker et al., 2009). ER, progesterone receptor (PR), and ERBB2 expression (negative/positive) was defined at the transcriptional level using gene expression data of *ESR1*, *PGR*, and *ERBB2* respectively, as previously described (Lehmann et al., 2011).

Correlations between tumor groups and clinicopathological features were analyzed using the t-test or the Fisher’s exact test (variables with 2 groups) when appropriate or one-way analysis of variance (ANOVA; variables with more than 2 groups). Metastasis-free survival (MFS) was calculated from the date of diagnosis until the date of distant relapse. Follow-up was measured from the date of diagnosis to the date of last news for event-free patients. Survivals were calculated using the Kaplan-Meier method and curves were compared with the log-rank test. All statistical tests were two-sided at the 5% level of significance. Statistical analysis was done using the survival package (version 2.30) in the R software (version 2.15.2; <http://www.cran.r-project.org/>). We followed the reporting REcommendations for tumor MARKer prognostic studies (REMARK criteria) (McShane et al., 2005).

Supplementary References:

- Ahmed, S. M., Theriault, B. L., Uppalapati, M., Chiu, C. W., Gallie, B. L., Sidhu, S. S., and Angers, S. (2012). KIF14 negatively regulates Rap1a-Radil signaling during breast cancer progression. *J Cell Biol* 199, 951-967.
- Bertucci, F., Finetti, P., Colpaert, C., Mamessier, E., Parizel, M., Dirix, L., Viens, P., Birnbaum, D., and Van Laere, S. (2015). PDL1 expression in inflammatory breast cancer is frequent and predicts for the pathological response to chemotherapy. *Oncotarget*.
- Charafe-Jauffret, E., Ginestier, C., Monville, F., Finetti, P., Adelaide, J., Cervera, N., Fekairi, S., Xerri, L., Jacquemier, J., Birnbaum, D., and Bertucci, F. (2006). Gene expression profiling of breast cell lines identifies potential new basal markers. *Oncogene* 25, 2273-2284.
- Irizarry, R. A., Hobbs, B., Collin, F., Beazer-Barclay, Y. D., Antonellis, K. J., Scherf, U., and Speed, T. P. (2003). Exploration, normalization, and summaries of high density oligonucleotide array probe level data. *Biostatistics* 4, 249-264.
- Lehmann, B. D., Bauer, J. A., Chen, X., Sanders, M. E., Chakravarthy, A. B., Shyr, Y., and Pietenpol, J. A. (2011). Identification of human triple-negative breast cancer subtypes and preclinical models for selection of targeted therapies. *J Clin Invest* 121, 2750-2767.
- McShane, L. M., Altman, D. G., Sauerbrei, W., Taube, S. E., Gion, M., and Clark, G. M. (2005). REporting recommendations for tumour MARKer prognostic studies (REMARK). *Br J Cancer* 93, 387-391.
- Parker, J. S., Mullins, M., Cheang, M. C., Leung, S., Voduc, D., Vickery, T., Davies, S., Fauron, C., He, X., Hu, Z., *et al.* (2009). Supervised risk predictor of breast cancer based on intrinsic subtypes. *J Clin Oncol* 27, 1160-1167.
- Ross, D. T., and Perou, C. M. (2001). A comparison of gene expression signatures from breast tumors and breast tissue derived cell lines. *Dis Markers* 17, 99-109.
- Sabatier, R., Finetti, P., Cervera, N., Tallet, A., Benchalal, M., Houvenaeghel, G., Jacquemier, J., Birnbaum, D., and Bertucci, F. (2011). Gene expression profiling and its utility in prediction of local relapse after breast-conserving therapy in early breast cancer. *Cancer Genomics Proteomics* 8, 199-209.
- Vizcaino, J. A., Csordas, A., Del-Toro, N., Dianes, J. A., Griss, J., Lavidas, I., Mayer, G., Perez-Riverol, Y., Reisinger, F., Ternent, T., *et al.* (2016). 2016 update of the PRIDE database and its related tools. *Nucleic Acids Res* 44, D447-456.